

An assessment of ocean alkalinity enhancement using aqueous hydroxides: kinetics, efficiency, and precipitation thresholds

Mallory C. Ringham¹, Nathan Hirtle¹, Cody Shaw¹, Xi Lu¹, Julian Herndon^{2,3}, Brendan R. Carter^{2,3}, Matthew D. Eisaman^{4,5}

¹Stony Brook University, Stony Brook, NY, USA

²Cooperative Institute for Climate Ocean and Ecosystem Studies, University of Washington, Seattle, USA

³Pacific Marine Environmental Laboratory, National Oceanic and Atmospheric Administration, Seattle, WA, USA

⁴Department of Earth & Planetary Sciences, Yale University, New Haven, CT, USA

⁵Yale Center for Natural Carbon Capture, Yale University, New Haven, CT, USA

Correspondence to: Mallory Ringham (mallory.ringham@stonybrook.edu); Current address: Ebb Carbon Inc., San Carlos, CA, USA

Abstract

Ocean alkalinity enhancement (OAE) is an approach to marine carbon dioxide removal (mCDR) that leverages the large surface area and carbon storage capacity of the oceans to sequester atmospheric CO₂ as dissolved bicarbonate (HCO₃⁻). One OAE method involves the production of an acid (HCl) and a base (NaOH) from seawater, the return of the base to the ocean, and the removal or neutralization of the acid. The resulting increase in seawater pH and alkalinity causes a shift in dissolved inorganic carbon (DIC) speciation toward carbonate and a decrease in the surface-ocean pCO₂. The shift in the pCO₂ results in enhanced net uptake of atmospheric CO₂ by the seawater due to gas exchange. In this study, we systematically test the efficiency of CO₂ uptake in seawater treated with NaOH at aquaria (15L) and tank (6000L) scales to establish operational boundaries for safety and efficiency in advance of mesocosm studies and scaling up to field experiments. CO₂ equilibration occurred on order of weeks to months, depending on circulation, air forcing, and air bubbling conditions within the test tanks. An increase of ~0.7-0.9 mol DIC/ mol added alkalinity (in the form of NaOH) was observed through analysis of seawater bottle samples and pH sensor data, consistent with the value expected given the values of the carbonate system equilibrium calculations for the range of salinities and temperatures tested. Mineral precipitation occurred when the bulk seawater pH_T (total scale pH) exceeded 10 and $\Omega_{\text{aragonite}}$ exceeded 30. This precipitation was dominated by Mg(OH)₂ over hours to 1 day before shifting to CaCO_{3, aragonite} precipitation. These data, combined with models of the dilution and advection of alkaline plumes, will allow for estimation of the amount of carbon dioxide removal expected from OAE pilot studies. Future experiments should better approximate field conditions including sediment interactions, biological activity, ocean circulation, air-sea gas exchange rates, and mixing-zone dynamics.

Keywords

Ocean Alkalinity Enhancement (OAE); marine carbon dioxide removal (mCDR); ocean carbon dioxide removal (ocean CDR)

1 Introduction

The Sixth Assessment Report of the Intergovernmental Panel on Climate Change reported that in addition to a drastic decrease in CO₂ emissions, active removal of 5-15 Gt of atmospheric CO₂ per year by 2100 is necessary to constrain average global warming to less than 1.5 - 2 °C (noting that the magnitude of carbon removals varies by

42 climate scenario: IPCC, 2022; Rogelj, 2018). A wide variety of negative emissions technologies (NETs) are under
43 development to meet this enormous challenge (Minx et al., 2018; NASEM, 2019; NASEM, 2021; Rueda et al.,
44 2021; Vitillo et al., 2022).

45 A suite of promising approaches to CO₂ removal termed ocean or marine carbon dioxide removal (ocean CDR or
46 mCDR, respectively) leverage the enormous surface area and carbon storage capacity of the ocean (Boettcher et al.,
47 2019; NASEM, 2021). Ocean alkalinity enhancement (OAE) is an mCDR method that aims to store atmospheric
48 CO₂ in a dissolved phase in the ocean as bicarbonate ions (HCO₃⁻), thereby accelerating a natural planetary CO₂
49 regulation mechanism, the carbonate-silicate cycle (Berner, 1983; Isson et al., 2020). OAE has the potential to scale
50 to gigatons of CO₂ removal per year (He and Tyka, 2023), but development of this approach requires careful
51 consideration of: the methods and materials used to source and process alkalinity; the form and method of delivery
52 of alkalinity to the surface ocean (for example, aqueous or solid phase); and selection of appropriate geographic sites
53 for alkalinity dispersal (Oschlies et al., 2023). OAE methods under exploration include: mining and crushing
54 alkaline minerals (e.g., olivine, basalts) to be spread via ship or in coastal environments (e.g., beach restoration, or
55 salt marsh distribution) (Feng et al., 2017; Köhler, Hartmann, and Wolf-Gladrow, 2010; Monserrat et al., 2018;
56 Rigopoulos et al., 2018); the mining or industrial production of Mg(OH)₂ or mining CaCO₃ and calcining it to CaO
57 or Ca(OH)₂, with the Mg(OH)₂ or Ca(OH)₂ spread via ship or coastal outfall pipe (Harvey, 2008; Ilyina et al., 2013;
58 Kheshgi, 1995; La Plante, 2023; Moras et al., 2022; Nduagu, 2012; Rau, 2008; Renforth and Henderson, 2017;
59 Shaw, 2022); and the electrochemical conversion of saltwater into aqueous hydroxides and dispersal via coastal
60 outfalls (de Lannoy et al., 2018; Eisaman et al., 2018; Lu et al., 2022; Tyka, Van Arsdale, and Platt, 2022; Eisaman
61 et al., 2023; Eisaman, 2024).

62 Many of these approaches and technologies are at a nascent stage and we must move quickly to quantitatively test
63 and characterize their performance to determine which, if any, justify larger-scale deployment. The electrochemical
64 conversion of salt (NaCl) into aqueous alkalinity (NaOH) has many potential advantages in scaling considerations,
65 including simplified distribution of a liquid product to the ocean, avoidance of mining and the transportation of the
66 alkalinity source over long distances, and avoidance of potentially harmful impurities present in mined alkalinity
67 sources (NASEM, 2021; Caserini, Storni, and Grosso, 2022).

68 Total alkalinity (TA) is defined as the excess of proton acceptors over proton donors in an aqueous solution (Eq. 1),
69 where ellipses represent neglected acids and bases (Dickson 1981; Dickson 1992; Wolf-Gladrow et al., 2007). A
70 higher TA value for a seawater sample indicates that it has a higher buffering capacity than a sample with a lower
71 TA value.

$$72 \quad \text{TA} = [\text{HCO}_3^-] + 2 [\text{CO}_3^{2-}] + [\text{B}(\text{OH})_4^-] + [\text{OH}^-] + [\text{HPO}_4^{2-}] + 2 [\text{PO}_4^{3-}] + \dots - [\text{H}^+] - [\text{HSO}_4^-] - \dots \quad (1)$$

73 Most of the OH⁻ from NaOH addition rapidly reacts with other molecules in seawater, but Eq. (1) is formulated so
74 the total remains unchanged through these reactions. From Eq. (1), we see the additional OH⁻ in a treated seawater
75 solution corresponds to a salt solution with increased alkalinity relative to the starting salt solution. The OH⁻ reacts
76 with and consumes free H⁺, thereby increasing the seawater pH. The OH⁻ also accepts protons from bicarbonate and
77 the carbonic acid formed from the reaction with CO₂ and H₂O, resulting in a shift of the dissolved inorganic carbon
78 (DIC) speciation towards carbonate according to the net reactions:



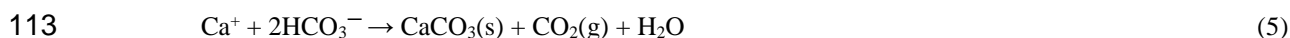
81 The concentration of dissolved CO₂ gas (CO_{2, aq}) in this alkalinity-enhanced seawater is less than it would be if it
82 were in equilibrium with atmospheric CO₂ (Equation 2b). Over the longer timescale required for air-sea gas
83 exchange - weeks to months (Wang et al., 2023) or months to years (He and Tyka, 2023) depending on location - the
84 disequilibrium in the surface ocean resulting from the alkalinity addition drives the invasion of atmospheric CO₂

85 into seawater (or lessens the outgassing of CO₂ from the surface ocean to the atmosphere), where it reacts with
86 carbonate and is stored primarily in the stable bicarbonate phase (Jones et al., 2014; Bach et al., 2023; Renforth and
87 Henderson, 2017; Eisaman et al., 2023).



90 As net reaction (2b) takes significantly longer than net reaction (2a), this process may have the potential to locally
91 and transiently mitigate the elevated *p*CO₂ and loss of carbonate ions associated with ocean acidification (NASEM,
92 2021; Cross et al., 2023; Butenschön et al., 2021) even though most of the carbonate ion that is initially produced (in
93 Eq. 2a) is eventually consumed (in Eq. 3b). After equilibrium has been reached OAE results in an increase in the
94 DIC in seawater on the order of ~0.7-0.9 moles of DIC per mole of NaOH added, depending on seawater conditions.
95 Following equilibration after OAE, the final pH and carbonate ion concentrations are slightly increased relative to
96 the initial values (He and Tyka, 2023).

97 It is possible that air-sea gas exchange will not completely drive the seawater *p*CO₂ to the initial unperturbed value
98 before the seawater sinks into the ocean interior and loses contact with the atmosphere for hundreds to thousands of
99 years. Therefore, the DIC anomaly relative to the alkalinity anomaly present when the seawater sinks into the ocean
100 interior may be used to assess the effective impact of the OAE for capturing atmospheric CO₂ on the 0-100 year
101 timescales that are most important for climate interventions. Deploying this OAE process in the ocean or coastal
102 waters will require an understanding of carbonate chemistry in seawater in the ocean volume under consideration, as
103 well as thresholds for safe operation. For example, at the point of alkaline dispersal where there is the maximum
104 change in seawater chemistry, the rate of alkalinity addition must be controlled relative to the rate of mixing and
105 dilution in the ocean to avoid the precipitation of Mg(OH)₂ or CaCO₃ (Hartmann et al., 2023; Moras et al., 2022).
106 While Mg(OH)₂ readily redissolves, an increase in turbidity due to precipitation may negatively affect marine
107 organisms (Bainbridge et al., 2018; Broderson et al., 2017). By contrast, CaCO₃ will generally not redissolve in the
108 surface ocean without biological mediation, and runaway precipitation, where alkalinity removed by precipitation
109 exceeds that added by the OAE treatment, can occur under conditions of increased aragonite saturation state and in
110 the presence of mineral nucleation sites in the water column (Moras et al., 2022). CaCO₃ precipitation could
111 counteract the intended effect of the OAE intervention by removing alkalinity from the surface ocean and releasing
112 CO₂ gas via Eq. 5 (Zeebe and Wolf-Gladrow, 2001):



114 Upon dispersal to the ocean through a coastal outfall pipe, the added alkalinity is advected and mixed away from the
115 point source, becoming increasingly diluted over time. Because the timescale for air-sea gas exchange and re-
116 equilibration described by Eq. (2) is longer than the characteristic timescale for dilution driven by tides, currents,
117 and weather, most of the CO₂ removal occurs far from the mixing zone. Dilution will spread the impacts over a
118 sufficiently broad area that it is unlikely that the impacts on the DIC distribution can be quantified using only direct
119 measurements given current instrument resolution and the typical dynamic range of natural variability (Wang et al.,
120 2023). In general, options for measurement, reporting, and verification (MRV) of OAE will therefore rely on (Ho et
121 al., 2023): experimentation in laboratory and mesocosm settings, such as the work we describe here, to establish
122 CO₂ removal dynamics under conditions of OAE; direct monitoring of the rate and characteristics of alkalinity
123 addition into seawater; monitoring the seawater carbonate and environmental chemistry in the immediate vicinity of
124 the outfall via sensors and sampling (Cyronak et al., 2023; Schulz et al., 2023); and ocean modeling to estimate
125 CDR beyond the range of direct detection (Fennel et al., 2023).

126 While some work has investigated various aspects of NaOH-based ocean alkalinity enhancement in microcosms
127 (Ferderer et al., 2022; Hartmann et al., 2023), and mesocosms (Groen et al., 2023), and other work has studied the

128 release of NaOH over natural coral reefs as a method of local ocean acidification mitigation (Albright et al., 2016), a
129 systematic characterization of the efficiency and kinetics of OAE as a function of key process parameters has not yet
130 been performed. Here we report the first tank-scale tests of OAE that use aqueous hydroxide (NaOH) to enhance the
131 alkalinity of natural seawater, a process that mimics OAE via electrochemical brine-to-alkalinity conversion. Our
132 experiments, conducted in 6,000 liter tanks using seawater pumped from Flax Pond on Long Island Sound in Stony
133 Brook NY, quantify the magnitude and timescale of the CO₂ removal from the air and storage as seawater DIC by
134 monitoring the air-seawater re-equilibration after an initial alkalinity perturbation. In addition, our use of both
135 laboratory-processed bottle samples and field-deployable sensors to measure and over-constrain the carbonate
136 chemistry response allows us to assess the suitability of certain sensing platforms for MRV. Finally, we investigate
137 safe thresholds for the rate and concentration of alkalinity addition to avoid: (1) the precipitation and redissolution of
138 Mg(OH)₂ that can lead to local, temporary increases in turbidity; and (2) the precipitation of CaCO₃, which partially
139 reverses the intended OAE effect by removing alkalinity from, and releasing CO₂ gas into, the surrounding seawater.

140 Using this approach, we address the following key questions:

141 (1) How much additional atmospheric CO₂ is stored in seawater as DIC in response to a given alkalinity
142 perturbation?

143 (2) What is the timescale for CO₂ removal from the air for these tanks, and how does it depend on the pH_T following
144 OAE and the magnitude of alkalinity enhancement?

145 (3) What are the conditions for Mg(OH)₂ precipitation upon addition of NaOH to seawater?

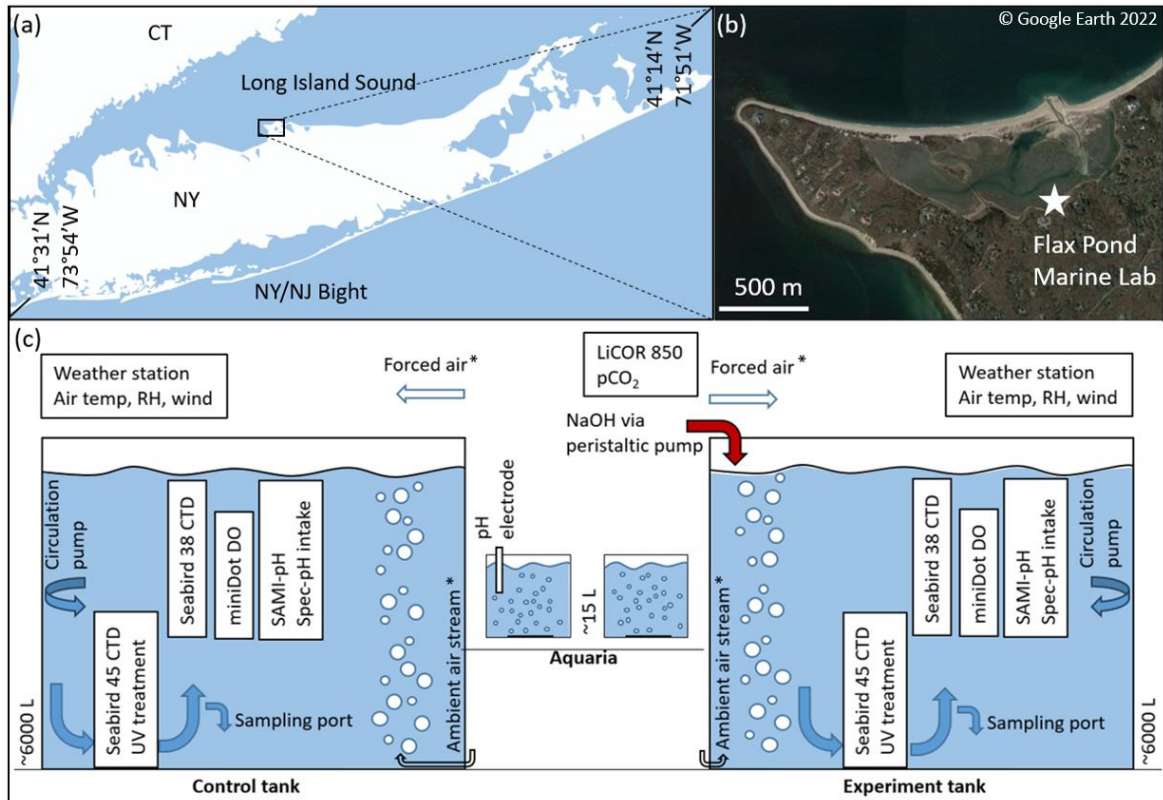
146 (4) What are the threshold values for pH_T and aragonite saturation state beyond which undesired CaCO₃
147 precipitation will occur?

148 Answering these questions is key to assessing the viability of this approach and to optimizing its eventual
149 deployment. The large tank experiments presented in this manuscript provide a stepping stone between bench-scale
150 experiments and in-situ mesocosms or field pilots, and are among the largest experiments that can be conducted with
151 a control seawater reference reservoir. Even if these experiments simply confirm stoichiometric and modeled
152 expectations, this is critical information in the design and implementation of OAE deployments. This work is a
153 necessary part of the growing scientific body that will allow for field trials to progress.

154 **2. Methods**

155 **2.1 Experimental procedure**

156 We investigated the carbonate chemistry changes resulting from the addition of NaOH_(aq) to natural seawater over
157 timescales ranging from 2 weeks to 2 months in a series of experiments at two scales: (1) two large (~6200 L)
158 indoor tanks, and (2) multiple 15 L aquaria (Fig. 1).



159

160 **Figure 1:** (a, b) Flax Pond Marine Laboratory is located on Long Island Sound, New York, USA (© Google Earth
 161 2022). (c) The ~6000 L control and experiment tanks were instrumented with a series of oceanographic sensors and
 162 sampled routinely for DIC/ TA analyses to allow for measurement of carbon uptake over time following an addition
 163 of alkalinity in the form of NaOH. The ~15 L aquaria were instrumented with standard glass pH electrodes and
 164 monitored with routine TA analyses. The Forced air* and Ambient air streams* indicate their use in some but not all
 165 experiments, as noted in later sections.

166 This study was conducted at the Flax Pond Marine Laboratory at Stony Brook University, NY. All experiments used
 167 natural seawater collected from Flax Pond, part of a 128-acre salt marsh tidal wetlands connected to the Long Island
 168 Sound. The surface areas of the tanks and aquaria were ~4.6 m² and ~0.1 m², respectively. The tanks had a diameter
 169 of 2.4 m, a total height of 1.52 m, and were typically filled to a height of ~1.35 m, allowing for a corresponding
 170 seawater volume of 6185 L. The aquaria had a diameter of 0.3 m and were typically filled to a height of ~0.23 m, for
 171 a total seawater volume of 15 L. The large tank volumes were chosen to limit interactions with walls while
 172 increasing the air-seawater boundary, and to lose a smaller fraction of their volume to evaporation. These tanks
 173 allow for in-situ oceanographic sensor deployment and frequent bottle sampling while retaining semi-controlled
 174 temperature, mixing, filtration, and biological control. The inherent limitations of these tank tests include limited air-
 175 sea interaction, unrealistic light levels and circulation, and biological responses that are not a perfect representation
 176 of natural seawater in the ocean, but serve as a stepping stone to mesocosm and eventual field experiments. On
 177 average, the large (~6,000 L) tank experiments took ~6.5 weeks after dosing with NaOH to reach 90% of the
 178 calculated or extrapolated asymptotic Δ DIC/TA addition ratio indicative of full air-seawater equilibrium, as will be
 179 discussed in Section 3. Therefore, in addition to the large tank tests, we conducted a series of smaller aquaria
 180 alkalinity additions to increase our capacity for experimental test cases. The limitations of the aquaria include
 181 limited sensor options, unrealistic circulation, and limited biological control. While it is expected that equilibration
 182 occurs more rapidly in the small aquaria than in the large tanks, the results from these cases should be similar after
 183 both experiment types have been allowed to fully equilibrate CO₂ across the air-seawater boundary. However, we

184 note that some variation is expected due to limited sensing and sampling options in the smaller aquaria and the
185 greater potential for biological growth in the large tanks over longer timescales.

186 2.1.1 Tank experiments

187 Seawater was pumped into the tanks at high tide through a series of sock filters to exclude macroscopic biology. The
188 tanks were then dosed to 40 ppm bleach (sodium hypochlorite) and the shock-treated seawater was allowed to
189 circulate through the tanks for ~1 day to limit biological growth. The seawater was then circulated through UV light
190 arrays to break down the bleach over ~1-2 weeks, as assessed by a standard Hach test kit for free chlorine. During
191 this period, seawater was pumped between the two large test tanks (~25 L/min) to increase mixing of the bleach and
192 to homogenize the tanks to similar initial conditions. For the remainder of each experiment, the seawater was
193 continually pumped through the UV sterilizers. Measurements of total alkalinity showed no significant differences
194 in the bulk seawater TA before and after the bleaching process in any experiment or control tank.

195 Oceanographic sensors and discrete daily bottle sampling, as described in Sections 2.2 and 2.3, respectively, were
196 deployed for carbonate chemistry analysis for several days prior to the alkalinity addition to understand the initial
197 baseline conditions in both tanks. Two submerged pumps were used for water circulation within each tank: the first
198 pump (Current eFlux DC Flow Pump, 210 GPH) cycled seawater through the UV arrays with an estimated
199 overturning time of the bulk tank on order of 1 day, and a second (Kedsum Submersible pump, 260 GPH), mounted
200 at an angle halfway down the tank wall, allowed for subsurface circulation within the tank to reduce the occurrence
201 of unmixed ‘dead zones’ and subsequent non-homogenous biological growth, as assessed visually on the surface of
202 the water and/or tank lining. Initial tank experiments were conducted with a still surface condition, i.e., with no
203 visible water movement across the surface of each tank. As experiments progressed, forced air movement was added
204 across the surface of each tank using a stationary fan with a wind speed of ~5 kph. This was done to control for
205 potential variations in the laboratory HVAC system and to potentially reduce the time to equilibration for the
206 experiments by increasing the rate of air-sea CO₂ equilibration. In later experiments, air was bubbled into the bottom
207 of each tank at a rate of ~30 L min⁻¹ with an estimated surface area of ~0.3 m², with a goal of further increasing the
208 rate of equilibration to allow for more rapid throughput of experiments. These variations are further discussed in
209 Section 2.4.

210 After baselining, one tank (referred to as the “experimental tank”) was dosed with enough 0.5 M NaOH (see
211 Supplementary Materials) to raise the bulk seawater pH_T to the target pH_T of interest for a given experiment, and the
212 same volume of DI water was added to the other tank (referred to as the “control tank”). NaOH additions were
213 typically dosed into the tank via peristaltic pump at a low enough rate (~50 mL/min) that a steady increase in bulk
214 tank pH_T was observed, but local pH_T measured just below the NaOH introduction never exceeded a pH_T of 9.0. A
215 pump (~25 L/min) was placed just below the NaOH stream to speed the mixing of NaOH into the bulk tank,
216 increase dilution from the point source, and to prevent the immediate precipitation of Mg(OH)₂ upon contact of the
217 NaOH with seawater. This pump was removed after the full volume of NaOH was mixed into the tank.

218 After the alkalinity addition, the tanks were left to equilibrate with the atmosphere and were monitored by sensors
219 and sampling as described in Sections 2.2 and 2.3. The tanks were indoors in the wet laboratory at Flax Pond Marine
220 Lab, such that temperature and CO₂ concentration were moderated by the building’s HVAC system, but varied
221 throughout days and seasons depending on other uses of the lab space. The experiments were concluded when the
222 observed pH_T or DIC (calculated from daily pH_T and frequent TA measurements) appeared to stabilize (e.g., ΔpH_T
223 ±0.05% or ΔDIC ±10 μmol kg⁻¹ per day) over several days, though we note that early experiments were terminated
224 before full equilibration. The continuous improvement of experimental methods during this study resulted in some
225 minor variations among the methods used for each experiment, including methods of NaOH dosing, tank circulation,
226 and biological control, as discussed where necessary in Section 3 and in the Supplementary Materials.

227 Seawater carbonate chemistry measurements were used to analyze the uptake of CO₂ in each tank, primarily relying
228 on calculations from the NOAA/PMEL DIC and TA analyses of bottle samples when available (described in Section
229 2.3) and using sensor pH_T and Stony Brook TA measurements for cross-verification or to fill in between discrete
230 DIC samples. DIC and TA data were normalized to the salinity at the start of a given experiment to account for
231 evaporation (Friis et al., 2003). Carbonate chemistry calculations were then performed using CO2SYS (Lewis and
232 Wallace, 1998), with Lueker et al. (2000) carbonate constants, Dickson (1990) for KSO₄, and Lee et al. (2010) for
233 total boron. Wherever possible, a combination of CRM analyses and comparisons between simultaneous pH_T sensor
234 and NOAA PMEL bottle samples were used to correct SAMI-pH and spectrophotometric pH_T sensor data for drift.

235 Changes in the seawater carbonate chemistry over time were analyzed with respect to shifts away from the baseline
236 within a single control or experiment tank, as well as with respect to the differences between the control and
237 experimental tanks. Henry's law and CO2SYS calculations were used to estimate the initial and final equilibration
238 condition of each tank experiment. LiCOR *p*CO_{2,atm} measurements were averaged across experiments to a
239 representative value (421 ± 14 ppm), which was used with the initial seawater temperature and salinity to estimate
240 *p*CO_{2,seawater} at the beginning of each experiment. The initial equilibrium DIC was estimated from a CO2SYS
241 calculation using the *p*CO_{2,seawater} and *n*TA_i. The final equilibrium *n*DIC was estimated from a CO2SYS calculation
242 using the same *p*CO_{2,seawater} and the *n*TA measured just after the NaOH addition, corrected for the linear increase in
243 salinity over the course of the experiment. The ratio of the expected Δ*n*DIC calculated at equilibrium with the
244 atmosphere to the addition of alkalinity provides a simple estimate of the expected CO₂ storage capacity for a given
245 experiment. The percent equilibration for each experiment was then estimated from the measured and expected
246 values for CAR.

247 2.1.2 Aquaria experiments

248 The large volume of tank experiments allowed for precise measurement of the seawater carbonate chemistry via
249 bottle sampling (1L each, sent to NOAA/PMEL for analysis) with high sampling frequency. To compliment these
250 measurements, we also performed a series of experiments in smaller aquaria (15 L each), which enabled a larger
251 number of replicates and a faster time to equilibrium when bubbled with air. A series of polycarbonate aquaria were
252 filled with 15 L of seawater taken from the large control tank just after the described bleaching and bleach
253 breakdown procedure was completed. NaOH was dosed into each aquaria to reach a targeted bulk pH_T, with a
254 corresponding volume of DI H₂O added to the control aquaria, and then the seawater was allowed to equilibrate with
255 atmospheric *p*CO₂ over days to weeks. The aquaria did not have either UV light arrays for biological control or
256 aquarium pumps for internal circulation. In most cases, the aquaria were bubbled with air (~4 L min⁻¹) via a standard
257 aquarium bubbling bar spanning the center diameter of each aquarium to reduce the equilibration time of these
258 experiments compared to the large tank experiments for all initial pH_T conditions investigated. There was no fine
259 control on air bubbling, but the surface area of all air bubbles in a given aquarium at any point in time was estimated
260 at ~0.01 m². No sensors were deployed in the aquaria due to their limited size, and seawater chemistry was
261 established via discrete pH_T and TA measurements (Sect. 2.2).

262 As shown in Eq. (6), we define the dimensionless 'Carbon-to-Alkalinity Ratio' (CAR) for our experiments as the
263 molar ratio of the increase in *n*DIC (in units of μmol/kg, normalized to the system's initial salinity to account for
264 evaporation) to the magnitude of the TA increase (ΔTA, in units of μmol/kg). *n*DIC_{equi} is the measured (via direct
265 titration) or calculated (via CO2SYS using measured TA and pH_T) DIC value that the system reached at the end of
266 an experiment (Pierrot et al., 2006; Van Heuven et al., 2011). Some experiments were left long enough to achieve
267 equilibration with atmospheric CO₂, but others were halted early. In these cases, a CO2SYS calculation was used to
268 estimate the DIC increase expected at equilibration given initial seawater conditions, and the difference between this
269 value and the final recorded *n*DIC_{equi} was used to estimate the overall percent equilibration for a given experiment.
270 Depending on experimental constraints described in later sections, *n*DIC_i may represent either: (1) the final *n*DIC
271 measured (via titration of bottle samples) or calculated (via CO2SYS using seawater TA and pH) in the control tank,

272 or (2) the ‘baseline’ $nDIC$ before the addition of NaOH to a given aquaria experiment, for cases where a
273 corresponding control case may not be available. Note that because we are reporting CAR values where the
274 measured DIC has reached or has been estimated at equilibrium, the CAR values we measure and report reflect the
275 ratio of ΔDIC to ΔTA that would be expected given sufficient time for air-sea exchange to reach equilibrium, and so
276 are equivalent to directly measuring the value of the “TA addition potential impact ratio” as defined by Wang et al.,
277 2023.

$$278 \quad \text{Carbon-to-Alkalinity Ratio (CAR)} = (nDIC_{\text{equ}} - nDIC_i) / \Delta TA \quad (6)$$

279 Not all aquaria experiments were directly comparable to the aquaria control. Seawater for one control aquarium was
280 collected in March 2023 and was monitored for pH_T and TA changes beginning in March 2023 and concluding in
281 May 2023. Seawater for the experimental aquaria was collected in three batches between March, April, and May
282 2023, with only 4-6 aquaria experiments running in parallel within each set of experiments due to space and
283 analytical throughput constraints. Because of this, the experiments started in March 2023 could be compared directly
284 to the control (target pH_T 8.3, 8.5, 8.5 still, and 8.7), but the rest of the experiments used different initial seawater
285 than the control aquaria. The CAR for each aquaria experiment was therefore calculated from changes in DIC and
286 TA between the initial ‘baseline’ condition and after the NaOH was added within a given aquarium, rather than
287 between the experiment and control cases.

288 With the exception of a single target pH_T 8.5 experiment, all aquaria were bubbled with ambient air, allowing for
289 rapid CO_2 exchange, and an optically clear lid was placed on each aquarium to reduce evaporation and splashing
290 onto nearby equipment. Some evaporation was evident from the rising TA throughout these experiments, but was
291 not resolvable within the resolution of a handheld salinometer used for these experiments, which ranged from values
292 of 30 – 31 during the experiments. Therefore, DIC and TA were not normalized to salinity in these cases.
293 Temperature was discretely recorded from a combination Ross pH electrode.

294 Each aquaria was gently stirred during the addition of NaOH to prevent $Mg(OH)_2$ precipitation. After the addition of
295 NaOH, the aquaria were allowed to equilibrate with atmospheric CO_2 . Similar to the large tank experiments, we
296 used Henry’s law and CO2SYS calculations to estimate the initial and final equilibration condition of each aquaria
297 experiment. The same average $pCO_{2,\text{atm}}$ of 421 ± 14 ppm was used with the initial seawater temperature and salinity
298 to estimate $pCO_{2,\text{seawater}}$ at the beginning of each experiment. The initial equilibrium DIC was estimated from a
299 CO2SYS calculation using this $pCO_{2,\text{seawater}}$ and TA_i . The final equilibrium DIC was estimated from a CO2SYS
300 calculation using the same $pCO_{2,\text{seawater}}$ and the TA measured just after the NaOH addition. The percent equilibration
301 for each experiment was then estimated between the measured and predicted values for $\Delta DIC / \Delta TA$. Due to the air
302 bubbling, most experiments approached equilibrium with the atmosphere within 1-7 days, with the exception of the
303 non-bubbled pH_T 8.5 experiment that took ~20 days. The surface water of this non-bubbled experiment was
304 stagnant, and the water was only mixed via stirring just before taking pH_T and TA samples.

305 2.2 Oceanographic sensors

306 Each tank was instrumented with a series of sensors placed halfway down the wall of the tank near the inlet of the
307 UV circulation pump. A Seabird 38 Digital Oceanographic Thermometer and Seabird 45 MicroTSG
308 Thermosalinograph continuously monitored seawater temperature and salinity, respectively. Dissolved oxygen was
309 measured by a PME miniDOT Logger at 10 min resolution. pH_T was monitored daily by a SAMI-pH (manufacturer
310 specified accuracy/precision ~ 0.003/0.001, though this accuracy is likely an underestimate of the uncertainty given
311 known challenges for the calibration of the pH_T measurements) and by a semi-automated spectrophotometric (spec-
312 pH) pH_T unit ($\sim \pm 0.0055/0.0004$) as described by Carter et al. (2013). CRM measurements were taken by each pH_T
313 system at the beginning and end of each experiment and were used alongside discrete samples of DIC and TA as
314 described in Section 2.3 to constrain the stability of each sensor. The SAMI-pH measurements were recorded at

315 ambient seawater temperature and corrected for in-situ salinity as recorded by the Seabird Thermosalinograph
316 following best practices from the manufacturer. The spec-pH_T analyses occurred in a jacketed cuvette held at 20 °C
317 (regulated via water bath) and were corrected to the in-situ bulk tank temperature and salinity as recorded by the
318 Seabird Thermometer and Thermosalinograph. Both the SAMI-pH and spec-pH_T rely on spectrophotometric
319 analysis of metacresol purple indicator dye, which allows for pH_T measurement within the pH_T range of
320 approximately 7 to 9. For experiments in which enough NaOH was dosed into seawater to raise pH_T above these
321 limits, a Thermo Scientific Orion ROSS Ultra pH/ATC Triode combination electrode (8157BNUMD) was used to
322 monitor pH_{NBS} at the surface of the tank (± 0.01 precision), which was then converted to pH_T for comparison with the
323 other pH_T measurement systems.

324 A LiCOR LI-850 sensor was used to analyze atmospheric *p*CO₂ ($\pm 1.5\%$ accuracy) above the tanks. The inlet to this
325 sensor was periodically moved between tanks to ensure that atmospheric *p*CO₂ in the vicinity of the control and
326 experiment tanks was the same. AcuRite Iris weather stations were mounted on the side of each tank to monitor air
327 temperature (± 2 °C), relative humidity ($\pm 3\%$), and air speed (± 0.8 m s⁻¹). All data were compiled on an hourly basis
328 in a custom R package.

329 **2.3 Discrete sampling**

330 Two types of discrete sampling were used to constrain carbonate chemistry throughout these experiments. First, 500
331 mL of seawater was collected and preserved from each tank, typically on a daily basis, and as frequently as hourly
332 during the addition of NaOH, following best practices laid out by Dickson (2007) including overflowing of the
333 sample bottles during collection and addition of 0.2 mL of saturated mercuric chloride (HgCl₂) as a preservative.
334 These bottle samples were analyzed for DIC and TA at NOAA Pacific Marine Environmental Laboratory
335 (NOAA/PMEL). DIC concentrations were measured using a coulometer (UIC Inc.) and Single Operator
336 Multiparameter Metabolic Analyzer (SOMMA) (Johnson et al., 1985). TA was determined by an open-cell
337 acidimetric titration (Dickson et al. SOP 3b, 2007). The accuracy of DIC and TA measurements was assessed with
338 Certified Reference Materials (CRMs, supplied by the Dickson laboratory at Scripps Institution of Oceanography),
339 and overall uncertainty for both DIC and TA was typically $\pm 0.1\%$ (~ 2 $\mu\text{mol/kg}$).

340 In addition, discrete seawater samples were analyzed for TA via open-cell potentiometric titration at Stony Brook
341 University. A Thermo Scientific Orion ROSS Ultra pH/ATC Triode combination electrode (8157BNUMD),
342 calibrated using three buffer solutions (pH_{NBS} 4.01, 7, and 10.01) was used to track the titration of a ~ 20 mL
343 seawater sample with a dilute HCl solution (~ 0.1 M in 0.7 M NaCl, calibrated daily with CRM or a secondary
344 seawater standard) following a modified Gran titration procedure using a Kloehe digital syringe pump (Song et al.,
345 2020; Wang and Cai, 2004). The precision of TA measurements was $\sim \pm 5$ -10 $\mu\text{mol/kg}$. This TA data was corrected
346 to that of the bottle samples analyzed via titration at NOAA PMEL where available (see Supplementary Materials).

347 There are several differences between the aquaria experiments and the larger tank experiments. First, the aquaria
348 experiments were monitored daily to every few days by discrete measurement of TA at Stony Brook University and
349 pH_{NBS} via Thermo Scientific Orion ROSS Ultra pH/ATC Triode combination electrode (8157BNUMD) (± 0.01
350 precision), which was then converted to pH_T and corrected against the other pH_T sensor systems via occasional
351 bottle samples for DIC and TA analysis at NOAA PMEL. Variations between these experiments are noted in
352 Section 3 where necessary and in the Supplementary Materials.

353 Samples of mineral precipitation were collected as follows: In the tank pH_T 10.3 case, discrete samples of the
354 precipitate were collected at seven different times after the bulk pH_T value reached 10.3 (0h, 3h, 24h, 49h, 71h,
355 145h, 167h - see Fig. 6) for XRD and SEM analysis. At each timepoint, 0.5 – 1 L seawater was collected from the
356 tank sampling port and was vacuum filtered through a 0.45 μm Whatman GF/F filter via vacuum pump and the
357 solids were rinsed with DI water 3 times to remove NaCl. The precipitate was dried in an oven at 90 °C, then

358 crushed into a uniform powder via mortar and pestle. Samples were analyzed via Hitachi 4800 Scanning Electron
359 Microscopy (SEM) (5 kV) and Rigaku SmartLab X-ray Diffraction (XRD) (Cu K α , 1.5406 Å, 10 - 100° 2 θ at
360 4°/min) at Brookhaven National Laboratory at the Materials Synthesis and Characterization Facility of the Center
361 for Functional Nanomaterials. We note that material that settled to the bottom of the large tanks was not directly
362 collected, and that only a subset of precipitation was collected at each time point, such that later timepoints may
363 include solids that had precipitated at the beginning of the experiment. Mineral samples from aquaria experiments
364 were collected less frequently due to the volume of seawater required. If precipitation had visibly settled at the
365 bottom of the aquaria, this material was stirred into the water column before sampling from the center of the aquaria.
366 The filtered seawater was immediately analyzed for TA and pH via Ross electrode because the heightened pH was
367 out of the range of spectrophotometric methods. Bottle samples of filtered seawater were not able to be analyzed at
368 NOAA PMEL due to the continued precipitation of CaCO₃ after filtration and preservation.

369 **3 Results and Discussion**

370 **3.1 Large tank experiments**

371 A summary of the range of oceanographic variables measured by sensors and bottle samples, calculated via
372 CO2SYS, or extrapolated to equilibration conditions during the large tank experiments is provided in Table 1. This
373 summary includes 6 experiments including 3 targeting pH_T 8.5 (still surface water, with forced air, and with forced
374 air and air bubbling) and one (each) targeting pH_T values of 8.7 (still surface water), 9.5 (with forced air and air
375 bubbling), and 10.3 (still surface water). In two early experiments in which bulk pH_T was raised from the initial
376 condition to 8.3 and to 8.7, the initial pH_T and TA varied between the control and experiment tanks as seawater was
377 pumped from multiple reservoirs and unevenly distributed between the tanks. The experiments were subsequently
378 refined to allow for several days of cross-pumping between tanks to homogenize the control and experiment
379 seawater before NaOH was added at the start of an experiment. More details on experimental variations and a larger
380 summary table are available in the Supplementary Materials. While the initial seawater conditions were similar
381 between the control and experiment tanks, we note that these cases are not entirely comparable after the termination
382 of cross-pumping between tanks and the subsequent addition of alkalinity. While tanks were initially bleached,
383 eventually some biological growth was noted in each tank with potential differences in spatial and temporal
384 distribution as well as species and community differences. Herein, we assume that differences between the control
385 and experiment cases are due to the addition of alkalinity alone, but we note that characterization of other potential
386 confounding factors is a subject for future work.

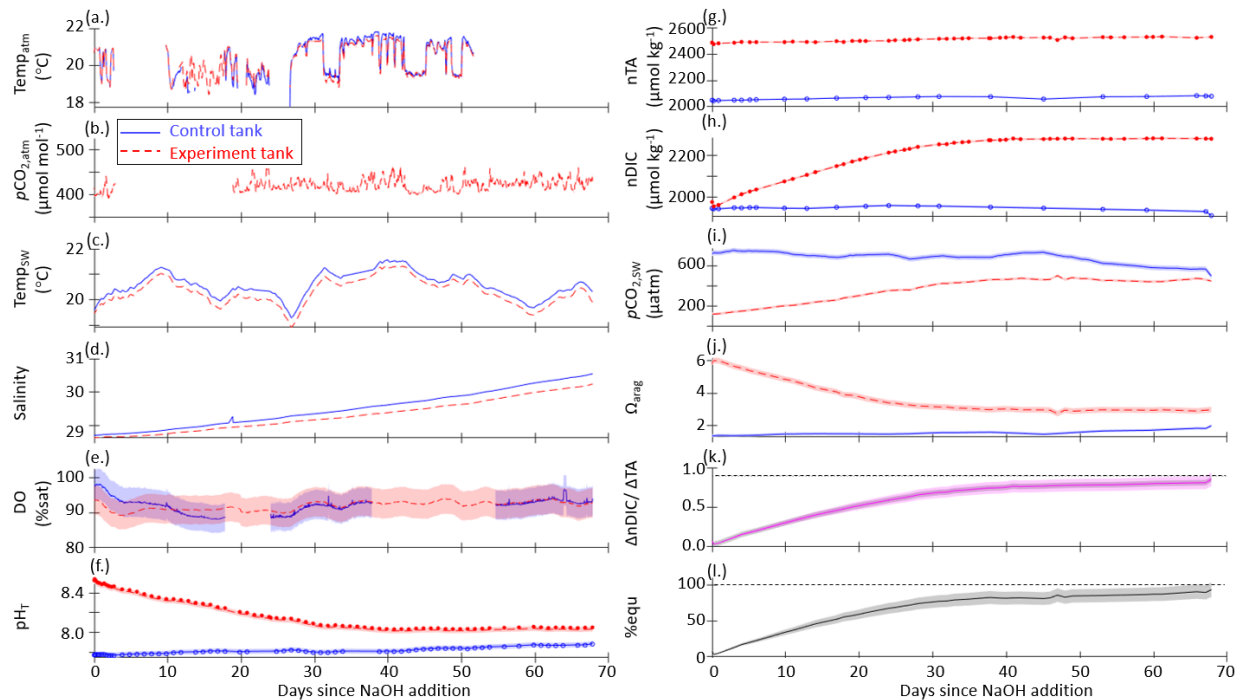
387 The initial pH_T, TA, and DIC varied across experiments as seawater was collected between March 2022 and May
388 2023, ranging from pH_T 7.66 (December 2022) – 7.95 (May 2023), TA 2001 (May 2023) – 2176 (March 2023)
389 $\mu\text{mol/kg}$, and DIC 1847 (May 2023) – 2021 (March 2023) $\mu\text{mol/kg}$. Both measured and CO2SYS -calculated DIC
390 and TA values were normalized to salinity to account for evaporation, which drove salinity increases ranging from
391 0.2 – 7.1 across these experiments.

392 In all experiments, the absorption of atmospheric CO₂ began immediately after the NaOH addition, as determined by
393 decreasing pH_T and Ω_{arag} and increasing DIC and seawater $p\text{CO}_2$. nTA was fairly stable or increasing (+10 - 60 μmol
394 kg^{-1}) after the NaOH addition in all cases except the pH_T = 10.3 experiment, where nTA and DIC rapidly decreased
395 due to runaway CaCO₃ precipitation. A stable TA value is an indicator that no significant persistent mineral
396 precipitation (e.g., Mg(OH)₂ or CaCO₃) has occurred. In the absence of active mixing or bubbling, Mg(OH)₂
397 precipitation occurred immediately upon the introduction of NaOH to seawater, however the precipitation can be
398 rapidly dissolved by turbulence (i.e., pumping NaOH directly above a strong circulation pump and/or stream of air
399 bubbles). No CaCO₃ precipitation was observed in the tanks or aquaria for which the bulk seawater pH_T was <10.0.
400 The pH_T = 10.3 experiment was designed to induce CaCO₃ runaway precipitation, as described in Section 3.3.

401 Ω_{arag} ranged from 1.4 - 2.5 in the control tanks with minimal variation over the course of any given experiment.
 402 During the three experiments in which bulk pH_T was increased to ~ 8.5 , Ω_{arag} increased immediately to 6.0 - 6.3 at the
 403 peak of the experiments, before slowly decreasing to 2.8 - 3.0 as the seawater equilibrated with atmospheric CO_2 .
 404 For the bulk pH_T 9.5 experiment, Ω_{arag} increased to 20.2 and slowly decreased to 5.0 when the experiment was
 405 ended at full equilibration. Mineral precipitation was observed in the bulk pH_T 10.3 experiment, where Ω_{arag} was
 406 increased to 30.3 and rapidly (<1 week) fell to 5.2 after the addition of NaOH.

407 The results of one representative set of time-series measurements from the control and experiment tanks are shown
 408 in Figure 2 for the case where pH_T of the bulk experiment tank was raised to 8.5 then allowed to relax into
 409 equilibration with the atmosphere without the addition of surface air forcing or bubbling. Time-series plots for the
 410 other tank-scale experiments are available in the Supplementary Materials.

411



412

413 **Figure 2:** Time-series data for the case where pH_T of the bulk experiment tank was raised to 8.5 with no forced air
 414 flow and no bubbling (still surface) for control (blue, solid) and experiment (red, dashed) tanks: (a) continuously
 415 measured air temperature, (b) atmospheric $p\text{CO}_2$, (c) seawater temperature, (d) salinity, and (e) dissolved oxygen; (f)
 416 pH_T measured by the SAMI-pH (circles) and interpolated from the spec- pH_T (line), corrected to bottle sample and
 417 CRM data; (g) NOAA/PMEL-measured TA and (h) DIC from bottle samples and normalized to salinity; (i)
 418 seawater $p\text{CO}_2$ and (j) saturation state of aragonite (Ω_{arag}) calculated from interpolated nDIC and nTA data via
 419 CO2SYS; (k) the observed carbon uptake ratio (CAR) as $(n\text{DIC}_{\text{exp}} - n\text{DIC}_{\text{control}}) / \Delta\text{TA}_{\text{NaOH addition}}$ (solid) and the
 420 theoretical CAR (dashed) from a CO2SYS calculation using measured TA and the average $p\text{CO}_{2\text{atm}}$ to estimate the
 421 equilibrium change in DIC (dashed); (l) the percent equilibration estimated between the observed and theoretical
 422 CAR. Data gaps in panels a, b, and e are due to connectivity issues while offloading sensor data.

423 The ΔnTA and ΔnDIC values calculated between the control and experiment tanks are summarized in Figure 3
 424 where nTA and nDIC were interpolated between bottle samples measured at NOAA-PMEL, and/or were calculated
 425 via CO2SYS using sensor pH_T and TA measured at Stony Brook University corrected to less frequent NOAA-
 426 PMEL TA and DIC bottle samples. The ratio of the ΔnDIC to the addition of alkalinity in the form of NaOH, or

427 ΔnTA , is included in Figure 3 for all experiments except that of the bulk pH_T increase to 10.3. Neglecting
 428 experiments that were terminated before full equilibration, the final observed CAR ranged from 0.75 ± 0.04 to 0.87
 429 ± 0.08 (Table 1).

430 An anomalous event was noted in both the experiment and control cases for the target pH_T 8.5 experiment with
 431 forced air movement across the surface of the tank, wherein an increase in TA and DIC was noted around day 30 of
 432 the experiment. The cause of this event is unclear but could include biological changes in both tanks, the
 433 introduction of alkalinity from environmental contaminants, or the anomalous delayed release of alkalinity from
 434 suspended solids. This event was not observed in any other case, and highlights the importance of using controls to
 435 understand complex interactions in these experiments. A time-series including this event is available in the
 436 Supplementary Materials.

437 The initial CO2SYS-calculated $pCO_{2,seawater}$ was in all cases greater than the atmospheric $pCO_{2,seawater}$, indicating
 438 that the seawater was not fully equilibrated with the atmosphere at the time when NaOH was added, likely due to
 439 respiration and decomposition of biology removed during the bleaching step (Section 2.1), and as such, the tanks
 440 should outgas CO_2 . The initial equilibrium DIC estimated from a CO2SYS calculation using the $pCO_{2,seawater}$ and
 441 nTA_i was in all cases less than the initial $nDIC$ measured or calculated from nTA_i and $pH_{T,i}$ (by $29 - 108 \mu mol kg^{-1}$).
 442 These observations underscore the importance of having a control tank to capture natural dynamics of CO_2 ingassing
 443 and outgassing to ensure that changes in DIC attributed to OAE are correctly accounted for.

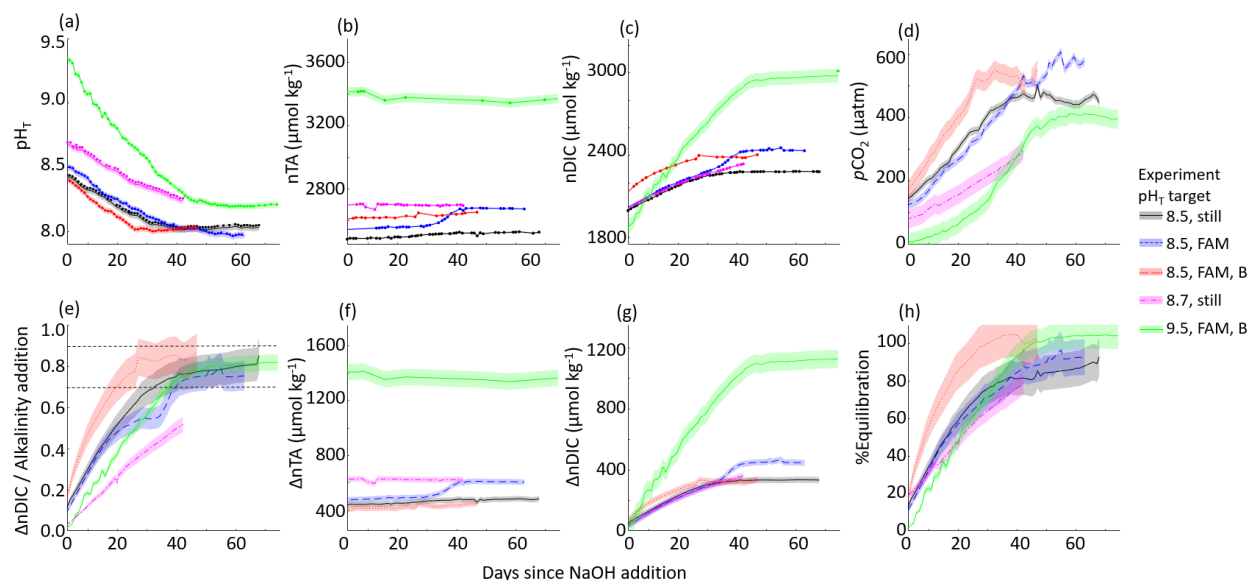
444 Within the series of experiments with a targeted pH_T of 8.5, the timeline to reach an estimated 90% CO_2
 445 equilibration decreased from 65 days (with internal circulation but still water at the surface of the tank), to 50 days
 446 (with the addition of forced air movement across the surface of the tank) to 22 days (with the addition of air
 447 bubbling). We note that only the two cases (targeted pH_T of 8.5 and 9.5) with the addition of air bubbling reached
 448 full equilibration with the atmosphere.

449 **Table 1:** Range of variables measured, calculated, or extrapolated in large tank experiments, where M denotes direct
 450 measurement, C denotes calculation via CO2SYS, and E denotes extrapolation to equilibrium conditions. Subscripts
 451 i and f refer to initial and final conditions, and ‘peak’ refers to the time point immediately after the addition of
 452 NaOH.

pH_T target	-	8.5		8.5		8.5		8.7		9.5		10.3	
Surface condition	-	Still		Forced Air		Forced Air and Air Bubbles		Still		Forced Air and Air Bubbles		Still	
Tank (C = control, E = experiment)	-	C	E	C	E	C	E	C	E	C	E	C	E
$\Delta TA = NaOH$ addition ($\pm 10 \mu mol/kg$)	M	0	409	0	462	0	375	0	626	0	1406	0	3305
Salinity _i (g/kg)	M	28.7	28.7	30.2	30.2	30.4	30.4	26.9	26.8	26.9	26.9	28.5	28.4
Salinity _f (g/kg)	M	30.5	30.2	37.3	36.6	34.7	33.7	27.6	27.6	29.0	29.2	28.6	28.6
$pH_{T,i}$ (± 0.005)	M	7.76	7.76	7.73	7.73	7.93	7.93	7.92	7.75	7.95	7.95	7.70	7.75
$pH_{T,peak}$ (± 0.005)	M	-	8.54	-	8.58	-	8.49	-	8.68	-	9.51	-	10.10
$pH_{T,f}$ (± 0.005)	M	7.88	8.05	7.85	7.99	7.99	8.01	7.84	8.26	8.01	8.21	7.75	9.52
nTA_i ($\pm 10 \mu mol/kg$)	M	2049	2049	2069	2069	2248	2248	2075	2075	2007	2007	2023	2025
nTA_{peak} ($\pm 10 \mu mol/kg$)	M	-	2458	-	2531	-	2623	-	2701	-	3414	-	5330
nTA_f ($\pm 10 \mu mol/kg$)	M	2080	2528	2235	2674	2246	2624	2095	2696	2014	3363	2041	1253

$nDIC_i$ ($\mu\text{mol/kg}$)	M	1944	1947	1957	1996	2082	2087	1897	1975	1852	1852	1928	1938
$nDIC_f$ ($\mu\text{mol/kg}$)	M	1908	2280	2084	2433	2027	2365	1937	2336	1832	2977	1947	720
$\Omega_{\text{aragonite},i}$	C	1.39	1.37	1.4	1.1	2.0	2.0	2.4	2.4	1.9	1.9	1.4	1.3
$\Omega_{\text{aragonite,peak}}$	C	-	5.9	-	6.0	-	6.2	-	8.8	-	19.3	-	30.3
$\Omega_{\text{aragonite},f}$	C	2.0	3.0	1.7	2.8	2.5	3.0	1.9	4.4	2.1	4.9	1.4	5.2
CAR_f	C	-	0.85 ± 0.04	-	0.75 ± 0.04	-	0.87 ± 0.08	-	0.52 ± 0.07	-	0.82 ± 0.09	-	-
$CAR_{\text{equilibrium}}$	E	-	0.89	-	0.85	-	0.85	-	0.84	-	0.81	-	-
% equilibration (time elapsed in days)	E	-	95 ± 10 (67)	-	92 ± 10 (63)	-	102 ± 12 (45)	-	79 ± 6 (42)	-	104 ± 7 (74)	-	(13)

453



454

455 **Figure 3:** Results of 5 tank-scale experiments in which enough NaOH was added to each tank to raise the bulk pH_T
456 to 8.3 – 9.7. pH_T decreased rapidly in all cases in which air bubbling sped equilibration with atmospheric CO_2 .
457 Results include: (a) measured pH_T , (b) measured nTA , (c) measured $nDIC$ or CO_2SYS calculated (for pH_T 9.5 case
458 only), (d) CO_2SYS -calculated pCO_2 , (e) the observed carbon uptake ratio (CAR) as $(nDIC_{\text{exp}} - nDIC_{\text{control}}) /$
459 $\Delta nTA_{\text{NaOH addition}}$ with horizontal dashed lines representing the expected range of 0.7-0.9 mol CO_2 uptake / mol NaOH
460 added to seawater, the change in (f) nTA and (g) $nDIC$ compared to the baseline measurements before the addition
461 of NaOH, and the percent equilibration estimated between the observed and theoretical CAR .

462 3.2 Aquaria experiments

463 Table 2 provides a summary of the range of oceanographic variables quantified for the aquaria experiments.

464 **Table 2:** Range of variables measured, calculated, or extrapolated in aquaria experiments, where M denotes direct
465 measurement, C denotes calculation via CO_2SYS , and E denotes estimation within specified equilibration
466 conditions. Subscripts i and f refer to initial and final conditions, and ‘peak’ refers to the time point immediately
467 after the addition of NaOH.

pH_T target	-	0 Control	8.3	8.5	8.5	8.7	9.3	9.5	9.7	9.9	10.0	10.1	10.2	10.3
---------------	---	--------------	-----	-----	-----	-----	-----	-----	-----	-----	------	------	------	------

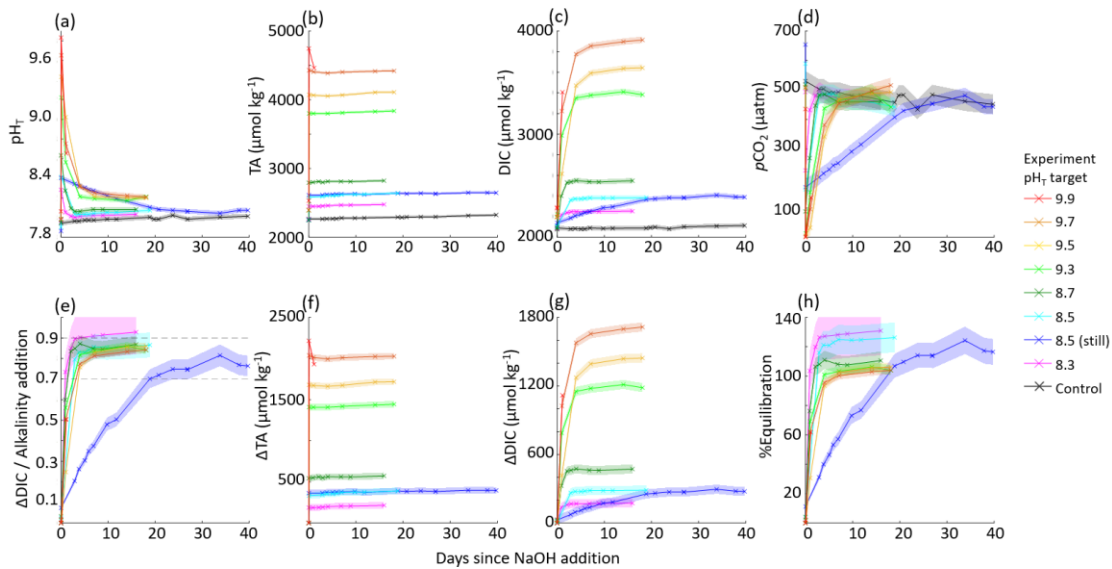
					Without air bubbles									
$\Delta TA = \text{NaOH}$ addition (± 10 $\mu\text{mol/kg}$)	M	0	187	331	362	543	1409	1679	2037	2216	2276	2504	2796	3829
$\text{pH}_{T,i}$ (± 0.1)	M	7.94	7.97	7.90	7.86	7.95	7.98	7.98	7.98	8.06	8.04	8.04	8.04	7.95
$\text{pH}_{T,\text{peak}}$ (± 0.1)	M	-	8.28	8.41	8.40	8.63	9.22	9.43	9.64	9.83	9.91	10.23	10.32	10.20
$\text{pH}_{T,f}$ (± 0.1)	M	8.06	8.03	8.07	8.11	8.08	8.21	8.20	8.23	8.65	8.96	8.72	9.46	7.99
TA_i (± 10 $\mu\text{mol/kg}$)	M	2265	2262	2250	2250	2250	2393	2393	2393	2531	2531	2531	2531	2250
TA_{peak} (± 10 $\mu\text{mol/kg}$)	M	-	2449	2582	2611	2793	3801	4072	4430	4748	-	-	-	4608
TA_f (± 10 $\mu\text{mol/kg}$)	M	2323	2476	2640	2645	2822	3837	4110	4420	4462	1702	1835	1537	2202
DIC_i ($\mu\text{mol/kg}$)	C	2089	2073	2091	2107	2070	2192	2192	2192	2282	2287	2287	2287	2067
DIC_f ($\mu\text{mol/kg}$)	C	2113	2246	2377	2382	2540	3372	3486	3877	3389	992	1244	671	2003
$\Omega_{\text{aragonite},i}$	C	2.1	2.2	1.9	1.8	2.1	2.34	2.4	2.4	2.9	2.8	2.8	2.8	2.1
$\Omega_{\text{aragonite},\text{peak}}$	C	-	4.2	5.5	5.5	8.1	19.5	23.1	27.0	29.8	30.2	30.9	32.4	38.9
$\Omega_{\text{aragonite},f}$	C	2.4	2.7	3.1	3.1	3.4	5.9	7.9	7.1	13.7	6.5	5.7	7.0	2.2
CAR_f	C	-	0.92 ± 0.10	0.87 ± 0.06	0.76 ± 0.05	0.87 ± 0.04	0.84 ± 0.02	0.86 ± 0.02	0.84 ± 0.02	0.50	-	-	-	-
$CAR_{\text{equilibrium}}$	E	-	0.69	0.67	0.64	0.77	0.80	0.80	0.80	0.81	-	-	-	-
% equilibration (time elapsed in days)	E	(40)	130 (16)	126 (18)	116 (40)	111 (16)	104 (18)	106 (18)	104 (18)	62 (1)	(1)	(1)	(1)	(16)
CaCO_3 precipitation?	M	-	No	No	No	No	No	No	No	No	Yes	Yes	Yes	Yes

468 The CAR ranged between 0.76 ± 0.05 and 0.92 ± 0.10 , excluding cases where mineral precipitation was evident and
469 for the pH_T 9.9 case where the experiment ended after one day due to a sensor logging failure. This wide range in
470 $\Delta DIC / \Delta TA$ is likely due to the lack of a control for aquaria experiments, limited number of TA samples collected
471 throughout these experiments (daily at best with no duplicates due to the limited volume), and the imprecision of
472 electrode-based pH_T measurements relative to the SAMI-pH and spec-pH_T based measurements used in the large
473 tank experiments.

474 The initial CO₂SYs-estimated equilibrium DIC was in all cases less than the initial DIC calculated from TA_i and
475 $\text{pH}_{T,i}$ (by 16 – 36 $\mu\text{mol kg}^{-1}$). This indicates that the seawater was not fully equilibrated with the atmosphere at the
476 time when NaOH was added, likely due to respiration and decomposition of biology removed during the bleaching
477 step (Section 2.1), and as such, the aquaria would be expected to outgas CO₂ if NaOH were not added. Absorption
478 of atmospheric CO₂ began immediately after the NaOH addition, as determined by decreasing pH_T . We note that
479 there are significant uncertainties in these equilibrium estimates leading to estimates of >100% equilibration. These
480 estimates would be better constrained with more continuous carbonate chemistry measurements, particularly
481 seawater and atmosphere $p\text{CO}_2$ throughout the experiments that would allow for more direct calculation of air-sea
482 CO₂ flux and equilibration, and finer control of bubbling and diffusion rates are necessary to define the timeline for
483 equilibration within the aquaria.

484 No CaCO₃ precipitation was observed in the tanks below a bulk seawater pH_T of 10.0, and TA remained stable in
485 each of these experiments with the exception of some increase driven by minor evaporation on the order of +2
486 $\mu\text{mol/kg}$ per day. Experiments where CaCO₃ precipitation was induced by increasing the starting pH_T to values
487 above 10 are discussed in Section 3.3.

488 The aquaria experiments with target pH_T from 8.3 – 9.9 are summarized in Figure 4.

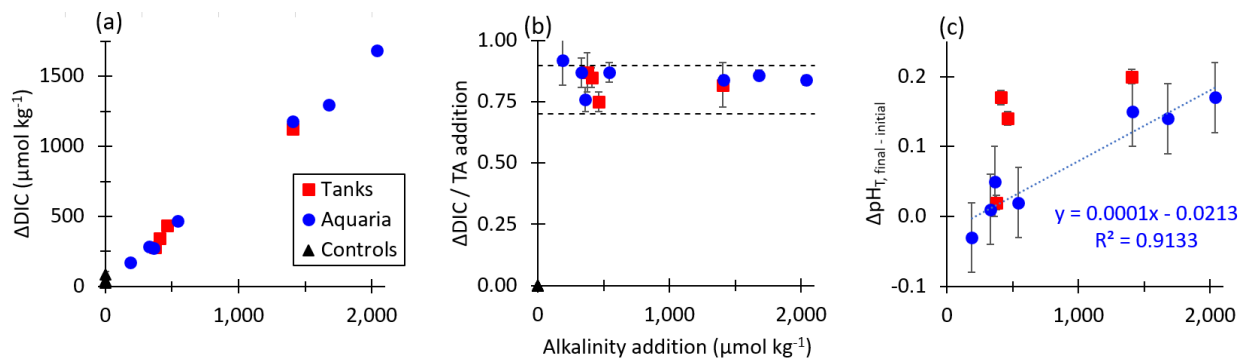


489

490 **Figure 4:** Results of 9 aquaria experiments in which enough NaOH was added to each aquaria to raise the bulk pH_T to 8.3 – 9.9. pH_T decreased rapidly in all cases in which air bubbling sped equilibration with atmospheric CO₂.
 491
 492 Results include: (a) measured pH_T, (b) measured TA, (c) CO₂SYN-calculated DIC, (d) CO₂SYN-calculated pCO₂,
 493 (e) the observed carbon uptake ratio (CAR) as $(DIC_{exp} - DIC_{baseline}) / \Delta TA_{NaOH\ addition}$ with horizontal dashed lines
 494 representing the expected range of 0.7-0.9 mol CO₂ uptake / mol NaOH added to seawater, the change in (f) TA and
 495 (g) DIC compared to the baseline measurements before the addition of NaOH, and the percent equilibration
 496 estimated between the observed and theoretical CAR.

497 In general, the large tanks and aquaria showed reasonable agreement in achieving values for CAR within the
 498 expected range of 0.7-0.9 (He and Tyka, 2023; Burt et al., 2021; Wang et al., 2023). While the use of aquaria
 499 bubbled with air to speed equilibration allowed for a greater range of data collection within a constrained experiment
 500 timeline, the quality of this data is limited by the lack of appropriate sensors to fit into these small 15 L aquaria,
 501 challenges with establishing control conditions, and fewer bottle samples due to the reduced quantity of seawater.
 502 However, while the large tanks allow for a larger range of oceanographic sampling and sensing techniques, it is
 503 more challenging to fully quantify mixing and circulation rates in the current large tank experimental setup.

504 Figure 5 shows the dependence of the equilibrium values of ΔDIC , CAR, and $\Delta pH_T = (pH_{final} - pH_{initial})$ as a function
 505 of the alkalinity addition for both tank and aquaria experiments in which the final percent equilibration for CO₂ was
 506 estimated at greater than 90%. Results for tank and aquaria experiments aligned well, with increasing ΔDIC for
 507 increasing alkalinity additions. The CAR was observed for all experiments to fall within the range expected for
 508 seawater with the temperature and salinity values used in these tests. As expected from calculations of the response
 509 of the seawater carbonate buffer system to additions of alkalinity, the final pH_T at equilibrium exceeded the pH_T of
 510 the control tank or aquaria at the same timepoint. That is, even once equilibrium in the alkalinity enhanced
 511 experiment tank had been reached, the ending pH value was slightly elevated relative to both the starting pH_T value
 512 and the pH_T of the control. While not all of these experiments resulted in complete equilibration, a line fit to the
 513 aquarium experiments has a slope of 0.0001 which is similar to the slope of the line that is expected from CO₂SYN
 514 when assuming complete equilibration with a 421 ppm CO₂ atmosphere.



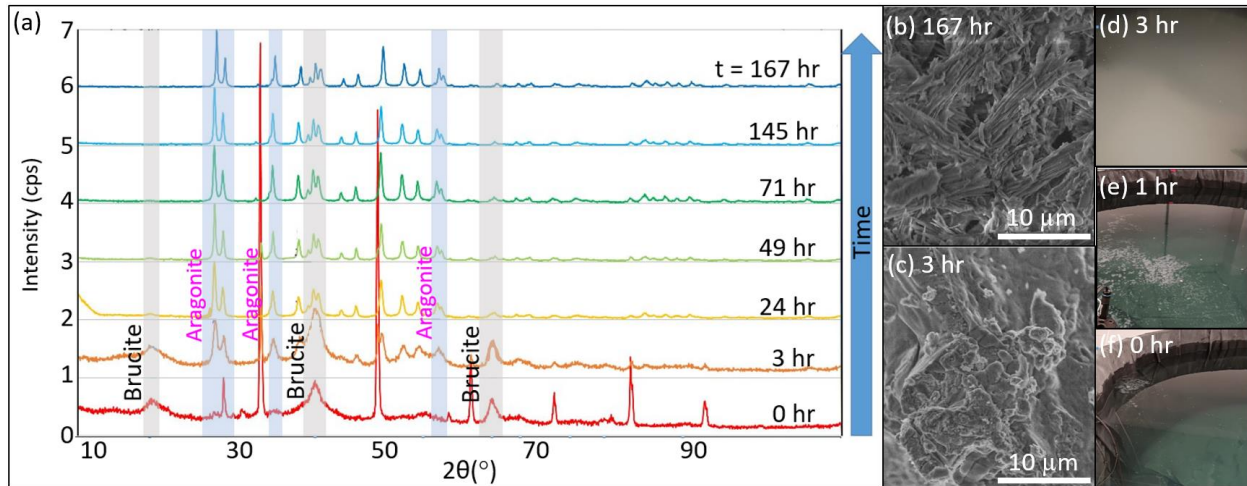
515
 516 **Figure 5:** (a) The change in final CO₂SYs-predicted DIC relative to the initial conditions for tank, aquaria, and
 517 control experiments increases with increasing NaOH additions for cases where the air-sea CO₂ equilibration was
 518 estimated at >90% at the termination of each experiment. (b) CO₂SYs-predicted CAR (Δ DIC / Alkalinity addition)
 519 at air-sea equilibrium conditions for tank, aquaria, and control experiments, with horizontal dashed lines
 520 representing the expected range of 0.7-0.9 mol CO₂ uptake / mol NaOH added to seawater. (c) The measured Δ pH_T
 521 = (pH_{final, experiment} - pH_{final, control}) increases with alkalinity addition for both tank and aquaria experiments.

522 3.3 Experiments exceeding the CaCO₃ precipitation threshold

523 While Mg(OH)₂ precipitation occurs immediately upon introduction of concentrated (i.e., ~0.5 M) NaOH to still
 524 seawater, it may be rapidly dissolved or avoided entirely by gentle mixing, including via the use of stirrers,
 525 circulation pumps, or air bubblers. This precipitation and redissolution happened rapidly enough that it was not
 526 identified in any TA or other variables measured in the aquaria and tank tests. However, in cases where enough
 527 NaOH was added to raise the bulk seawater pH_T to greater than 10.0 (i.e., in one large tank test with a target pH_T of
 528 10.3, and in 4 aquaria experiments ranging from pH_T 10.0-10.3), runaway precipitation of Mg(OH)₂ and CaCO₃ was
 529 observed. This was characterized by a sharp reduction in both TA and DIC and an increase in turbidity, and a
 530 continued depletion of DIC and slow removal of TA as atmospheric CO₂ from gas exchange was converted to
 531 additional CaCO₃. Runaway precipitation has been described as a condition in which more alkalinity is removed
 532 from seawater by mineral precipitation than was initially added until a new steady state is achieved (Moras et al.,
 533 2022; Hartmann et al., 2023; Suitner et al., 2023). This can significantly reduce the efficiency of OAE, and has
 534 implications for biological productivity, as increased turbidity may impact photosynthesis or predator-prey
 535 interactions.

536 Both XRD and SEM results of the mineral precipitation showed the dominance of Mg(OH)₂ precipitation
 537 immediately after the alkalinity addition and the corresponding increase in pH and $\Omega_{\text{aragonite}}$ (to a value of around 30),
 538 though this signal was partially obscured by the presence of other salts. The Mg(OH)₂ precipitation at this stage was
 539 thick, slurry-like, and difficult to appropriately rinse. Within hours of the NaOH addition, the runaway CaCO₃
 540 precipitation began, characterized by fine, light particulates in the water column and a sharp increase in turbidity.
 541 Within ~24 hours of the NaOH addition, most Mg(OH)₂ signals had disappeared, leaving only aragonite and calcite
 542 peaks in the XRD. The results of the XRD analysis for the tank experiment are summarized in Figure 7, and the
 543 aquarium experiment showed similar results. TA decreased throughout the precipitation of Mg(OH)₂ and CaCO₃,
 544 and was below that of the initial seawater within 24 hours of the NaOH addition. In the tank experiment, the initial
 545 TA (2025 μmol/kg) was raised by 3305 μmol/kg. Within 3 days the TA had decreased to 1583 μmol/kg and
 546 continued to decrease through the termination of the experiment to 1253 μmol/kg 10 days after the addition of
 547 NaOH. The DIC, which was initially measured to be 1938 μmol/kg, decreased to 720 μmol/kg by the end of the
 548 experiment. This experiment shows that runaway CaCO₃ can result in a significant loss of both efficiency of
 549 alkalinity dosing for OAE projects and of storage of carbon in the form of DIC. A figure of time-series data
 550 collected during the tank experiment is available in the Supplementary Materials.

551



552

553 **Figure 6:** (a) XRD analysis (top) of particulates filtered from seawater after the addition of enough NaOH to raise
 554 the bulk seawater pH_T to 10.3 showed mineral precipitation initially dominated by $\text{Mg}(\text{OH})_2$ before it was overtaken
 555 by $\text{CaCO}_{3,\text{arag}}$. The shaded grey vertical bars highlight peaks characteristic of brucite which typically disappear after
 556 24 hours, and the shaded blue bars represent several aragonite peaks which appear between 3 and 24 hours.
 557 Representative SEM images show (b) $\text{CaCO}_{3,\text{arag}}$ at the end of the experiment, and (c) $\text{Mg}(\text{OH})_2$ captured ~3 hours
 558 after the NaOH addition. Photographs of the tank experiment show seawater (d) ~3 hours after the NaOH addition,
 559 when runaway CaCO_3 precipitation became visually apparent, (e) during NaOH addition into still water (i.e.,
 560 without the use of stirrers, circulation pumps, or air bubblers to break up and redissolve $\text{Mg}(\text{OH})_2$), and (f) before
 561 NaOH addition.

562 In summary, the presence and duration of brucite precipitation upon addition of 0.5 M aqueous NaOH depends on
 563 the ratio of the NaOH addition rate to the local dilution rate in the receiving waters. Future research using flow
 564 through tanks could help identify thresholds below which brucite precipitation can be avoided or limited, and the
 565 immediate formation of $\text{Mg}(\text{OH})_2$ may be reversible, as also noted by Suitner et al. (2023) and Cyronak et al.
 566 (2023). At the given initial seawater conditions, the threshold for aragonite precipitation began at an Ω_{arag} of 30,
 567 corresponding to $\text{pH}_T > 10.0$, and continued as Ω_{arag} decreased to ~5.2. This threshold corresponded to an increase in
 568 TA of $>2270 \mu\text{mol}/\text{kg}$. The potential for runaway aragonite precipitation may be reduced by active mixing at the
 569 point of NaOH introduction, maintaining a mixing volume below bulk seawater pH_T of 10.0, and allowing for
 570 appropriate dilution in flow-through conditions, particularly on timescales of hours after alkalinity addition.

571 Characterization of runaway precipitation thresholds at varying temperatures, salinities, and suspended particulate
 572 conditions will allow for OAE implementation designs that best avoid this potential risk to OAE efficiency and
 573 ecosystem perturbation. We note that these results are only valid for open experiments using an aqueous hydroxide
 574 feedstock for alkalinity, and may not be comparable to bench-scale experiments such as closed bottle incubations,
 575 where increased surface area, edge effects, and sustained conditions of high Ω_{arag} may result in precipitation at
 576 different thresholds. We also note that we do not assume zero aragonite precipitation at conditions below the stated
 577 thresholds, but that potential precipitation is not readily detectable with our experimental setup. For example,
 578 heterogeneous CaCO_3 precipitation events, such as may occur on suspended sediments in the water column, have
 579 been suggested through characteristic changes in seawater TA/DIC ratios in cases of riverine inputs and bottom
 580 sediment resuspension (Bustos-Serrano et al., 2009; Wurgaft et al., 2016; 2021). Suspended sediments in the context
 581 of OAE project sites could influence OAE efficiency and the potential for runaway precipitation and should be
 582 included in future studies (Bach, 2023). The thresholds determined in this study are significantly higher than those
 583 of some mineral-based OAE studies, including precipitation after an increase in TA of $\sim 500 \mu\text{mol}/\text{kg}$ using CaO and

584 Ca(OH)₂ mineral additions (Moras et al., 2022). Hartmann et al. (2022) noted precipitation resulting from alkalinity
585 additions of >600 μmol/kg Mg(OH)₂, and found that aqueous alkaline solutions avoided carbonate precipitation
586 better than reactive alkaline particle additions to seawater. Suitner et al. (2023) suggested that alkalinity additions >
587 2000 μmol/kg could be achievable given sufficient dilution to avoid runaway precipitation. Together, these studies
588 highlight the need to expand research into runaway precipitation to characterize potential inefficiencies in OAE,
589 particularly in in-situ experiments to establish relationships applicable to ocean environments.

590 **5 Summary**

591 These results demonstrate that ocean alkalinity enhancement using aqueous sodium hydroxide in seawater results in
592 CO₂ removal from air at an efficiency of 0.75 (± 0.04) – 0.92 (± 0.10), with 90% equilibration typically achieved
593 within 7 - 9 weeks (still surface water with ~16 L/min subsurface circulation through UV arrays) to 3 - 5 weeks
594 (with the addition of ambient air bubbling into the bottom of each tank) of the initial addition when performed in
595 ~6000 L tanks with seawater-air contact areas of around 4.6 m². These results are in general agreement with ratios
596 noted in Burt et al. (2021), He and Tyka (2023), and Wang et al., (2023), and thus give no reason to doubt the air-sea
597 equilibrium dynamics used in these model based OAE studies. Here, uncertainties are driven by sensor precision and
598 temporal resolution in discrete DIC and TA sampling, the limited number of experiments with minimal
599 opportunities for duplicates or replicates, and poorly constrained data on mixing, circulation, and air bubbling rates.
600 Ongoing experiments seek to improve each of these conditions and should particularly focus on constraining the
601 movement of water within a given tank to improve air-sea equilibration estimates and to allow for better
602 extrapolation from tank to field experiments. In addition, a focus of ongoing and future work is to provide rate
603 estimates for the uptake of atmospheric CO₂ in response to an NaOH addition, allowing for fitting and extrapolation
604 of a shortened experiment to equilibration with the atmosphere. While the tank-to-atmosphere exchange rate is
605 unlikely to be generalizable to the ocean sea-to-air kinetics, it is essential information for the storage of high TA
606 solutions (which will be a common element of many OAE field trials) and for the subset of proposed approaches
607 that plan to conduct partial pre-equilibration of high-TA seawater mixtures before discharge (typically to avoid
608 creating high-pH environmental conditions).

609 We relied on several methods to constrain seawater carbonate chemistry. The tank-scale experiments primarily
610 relied on discrete (at most daily) DIC and TA sampling (NOAA PMEL), paired with daily measurements from
611 spectrophotometric pH systems (SAMI-pH and a semi-automated benchtop spec-pH system following Carter et al.
612 (2013)) and local TA measurements. With appropriate calibration or correction of the spec-pH systems relative to
613 CRM, there was no significant difference in carbonate calculations using the NOAA PMEL DIC-TA or spec-pH-
614 local TA pairings, though the latter case typically produced larger uncertainties. Aquaria experiments relied on a
615 standard glass pH electrode (at most daily, corrected to spectrophotometric systems) with discrete (at most daily) TA
616 measurements, which provided reasonable data relative to the tank experiments. As a result, ongoing tank-scale
617 experiments have limited the volume of discrete DIC and TA samples collected for analysis at NOAA PMEL to
618 allow for faster and less expensive monitoring via spec-pH and local TA titrations. However, we note that the major
619 limitation in this measurement pathway lies in the spec-pH method, which is typically limited to pH_T measurements
620 ranging from 7 – 9 for the meta-cresol purple indicator dye used. While our measurements retained some sensitivity
621 up to pH_T 9.5, such a method should typically be considered unreliable at these pH_T values, and we relied on
622 frequent correction to CRM and comparison with DIC/TA samples. Thymol blue is an alternative
623 spectrophotometric pH_T indicator dye with sensitivity over the higher pH_T conditions observed during these initial
624 trials and will be assessed for future experiments (Zhang and Byrne, 1996; Liu et al., 2006).

625 Aqueous NaOH with concentrations as high as 0.5 M can be added directly to turbulent seawater with only limited
626 observable precipitation of Mg(OH)₂. In these conditions this precipitated mineral rapidly redissolves on the
627 timescales of minutes to seconds. Improved control over the NaOH dosing rate (in our tank experiments, ~50 mL
628 NaOH/min) and the turbulence of the receiving water through metered flow through experiments will be valuable in

629 extrapolating to field conditions. This precipitation is detectable both visually and through turbidity measurements
630 and implies that straightforward measurement of pH and turbidity at the dispersal site can be used to adjust the
631 alkalinity dispersal rate according to local mixing conditions such that $\text{Mg}(\text{OH})_2$ precipitation is avoided and/or
632 redissolves when it occurs. No significant CaCO_3 precipitation was observed at $\text{pH} < 10.0$ or $\Omega_{\text{aragonite}} < 30.0$.
633 Runaway CaCO_3 precipitation was observed above these thresholds, where a massive precipitation and settling of
634 $\text{Mg}(\text{OH})_2$ and CaCO_3 solids results in less alkalinity in the overlying water than at the starting condition. pH and
635 turbidity sensing combined with discrete TA measurements could be used as a feedback signal for alkalinity dosing
636 into seawater to ensure that the local maximum thresholds at the dispersal location do not approach or exceed
637 conditions that promote significant CaCO_3 precipitation. We note that future investigations seeking to better
638 approximate field conditions should take into account seasonal and tidal shifts in temperature and salinity, and
639 varying conditions of suspended sediment in the water column, including that of aerial dust, terrestrial runoff, and
640 resuspended bottom sediments.

641 In these experiments, the seawater was filtered and bleach treated prior to experiments to limit biological growth,
642 and both tank and aquaria experiments were conducted indoors with limited light. Nevertheless, in most
643 experiments, biological growth was observed after a few weeks, including cyanobacteria and coccolithophores. A
644 series of experiments are underway to test the difference in CO_2 removal efficiency for two side-by-side tanks, both
645 of which are dosed with NaOH , but only one of which was bleached. Preliminary results show minimal difference
646 between the bleached and unbleached tanks, indicating these experiments are applicable to real-world conditions, at
647 least for regions with biological communities similar to that of Long Island Sound, but further investigation is
648 warranted.

649 A focus of future work is to consider the potential impact of electrochemical OAE on local ocean acidification
650 mitigation efforts. We note that in each constrained tank and aquaria experiment, the pH_T at equilibrium exceeds the
651 initial pH_T value prior to the addition of alkalinity (see Fig. 5c). A controlled release of alkalinity could theoretically
652 be configured to maintain a locally elevated pH_T value relative to pre-alkaline conditions, with potential uses in
653 aquaculture and hatchery environments.

654 These results provide clear and practical guidelines for MRV for OAE implementations employing aqueous
655 alkalinity. First, carbonate chemistry and turbidity measurements at the alkalinity dispersal location can ensure that
656 seawater parameters such as pH and $\Omega_{\text{aragonite}}$ remain within pre-determined safe bounds and that unwanted
657 precipitation is avoided. Second, for a given OAE deployment, where ocean models provide a reasonable certainty
658 about the fraction of the alkalinity plume remaining in the surface over weeks to months, the CO_2 removal efficiency
659 and timescale for air-seawater equilibration provided by our shallow-depth experiments can place an upper bound on
660 the amount of CO_2 removal expected from that OAE intervention. Expanding these studies from tank scale to
661 mesocosm and field experiments will be crucial to understanding biological impacts and constraining realistic air-
662 sea interactions in response to this type of OAE (Oschlies et al., 2023).

663 **Data availability**

664 Data are described in the manuscript and provided Supplementary Materials, which includes a .csv file with
665 processed sensor and sample time-series data at hourly resolution.

666 **Author contribution**

667 MDE and BRC designed the experiments and MCR carried them out with support from NH, CS, and XL. JH
668 provided support on experimental setup and instrumentation. MCR prepared the manuscript with contributions from
669 all co-authors.

670 **Competing interests**

671 MCR is Lead Oceanographer and Head of MRV at Ebb Carbon, Inc. MDE is Co-Founder and Chief Scientific
672 Advisor at Ebb Carbon, Inc.

673 **Acknowledgements**

674 We would like to than Stephen Abrams and Thomas Wilson at Stony Brook University Flax Pond Marine Lab for
675 technical assistance in experiment setup. We thank Chris Ikeda and Susan Curless of NOAA PMEL for support in
676 discrete sample analysis. We thank Mike Tyka for productive discussions. We thank Eyal Wurgaft for assistance in
677 TA titrations.

678 **Funding**

679 We acknowledge funding from The Grantham Foundation for the Protection of the Environment under the SEA
680 MATE (Safe Elevation of Alkalinity for the Mitigation of Acidification Through Electrochemistry) grant. In
681 addition, this research used the XRD facility of the Center for Functional Nanomaterials (CFN), which is a U.S.
682 Department of Energy Office of Science User Facility, at Brookhaven National Laboratory under Contract No. DE-
683 SC0012704. BRC and JH were funded through the Cooperative Institute for Climate, Ocean, and Ecosystem
684 Studies (CICOES) under NOAA Cooperative Agreement NA20OAR4320271 and supported by NOAA's PMEL.

685 **References**

- 686
687 Albright, R., Caldeira, L., Hoffelt, J., Kwiatkowski, L., Maclaren, J.K., Mason, B.M., Nebuchina, Y. et al.: Reversal
688 of ocean acidification enhances net coral reef calcification. *Nature*, 531, no. 7594: 362-365, 2016.
689 Bach, L.T.: The additionality problem of ocean alkalinity enhancement. *Biogeosciences Discussion*. [preprint], in
690 review, 2023
691 Bach, L. T., Gill, S.J., Rickaby, R.E.M., Gore, S., and Renforth, P.: CO₂ removal with enhanced weathering and
692 ocean alkalinity enhancement: potential risks and co-benefits for marine pelagic ecosystems. *Frontiers in*
693 *Climate*, 1, 7, 2019.
694 Bainbridge, Z., Lewis, S., Bartley, R., Fabricius, K., Collier, C., Waterhouse, J., Garzon-Garcia, A., Robson, B.,
695 Burton, J., Wenger, A., and Brodie, J: Fine sediment and particulate organic matter: A review and case study on
696 ridge-to-reef transport, transformations, fates, and impacts on marine ecosystems. *Marine Pollution Bulletin*
697 135, pp. 1205-1220. 2018
698 Berner, R. A., Lasaga, A.C., and Garrels, R.M.: Carbonate-silicate geochemical cycle and its effect on atmospheric
699 carbon dioxide over the past 100 million years. *Am. J. Sci.:(United States)* 283, no. 7, 1983.
700 Boettcher, M., Chai, F. Cullen, J., Goeschl, T., Lampitt, R., Lenton, A., Oschlies, A. et al.: High level review of a
701 wide range of proposed marine geoengineering techniques. *GESAMP Working Group Reports and Studies*, 41,
702 2019.
703 Broderson, K.E., Hammer, K.J., Schrammeyer, V., Floytrup, A., Rasheed, M.A., Ralph, P.J., Kühl, M., and Pederson,
704 O.: Sediment resuspension and deposition on seagrass leaves impedes internal plant aeration and promotes
705 phytotoxic H₂S intrusion. *Frontiers in Plant Science* 8. 2017
706 Burt, D.J., Fröb, F., & Ilyina, T.: The sensitivity of the marine carbonate system to regional ocean alkalinity
707 enhancement. *Frontiers in Climate* 3, 624075. 2021
708 Bustos-Serrano, H., Morse, J.W., & Millero, F.J.: The formation of whittings on the Little Bahama Bank. *Marine*
709 *Chemistry* 113, no. 1-2, pp. 1-8. 2009
710 Butenschön, M., Lovato, T., Masina, S., Caserini, S., and Grosso, M.: Alkalinization scenarios in the Mediterranean
711 Sea for efficient removal of atmospheric CO₂ and the mitigation of ocean acidification. *Frontiers in Climate* 3,
712 614537. 2021
713 Carter, B. R., J. A. Radich, H. L. Doyle, and A. G. Dickson.: An automated system for spectrophotometric seawater
714 pH measurements. *Limnology and Oceanography: Methods*, 11, no. 1: 16-27, 2013.

715 Caserini, S., Storni, N., & Grosso, M.: The availability of limestone and other raw materials for ocean alkalinity
716 enhancement. *Global Biogeochemical Cycles*, 36, e2021GB007246. <https://doi.org/10.1029/2021GB007246>,
717 2022.

718 Cross, J.N., Sweeney, C., Jewett, E.B., Feely, R.A., McElhany, P., Carter, B., Stein, T., Kitch, G.D., and Gledhill,
719 D.: Strategy for NOAA carbon dioxide removal research: A white paper documenting a potential NOAA CDR
720 science strategy as an element of NOAA's Climate Interventions Portfolio. NOAA Special Report. NOAA,
721 Washington, DC. DOI: 10.25923/gzke-8730. 2023

722 Cyronak, T., Albright, R., and Bach, L.: Chapter 4.5: Field Experiments, *State Planet Discuss.* [preprint],
723 <https://doi.org/10.5194/sp-2023-9>, in review, 2023.

724 de Lannoy, C.-F., Eisaman, M.D., Jose, A., Karnitz, S.D., DeVaul, R.W., Hannun, K., and Rivest, J.L.B.: Indirect
725 ocean capture of atmospheric CO₂: Part I. Prototype of a negative emissions technology. *International journal of*
726 *greenhouse gas control*, 70: 243-253, 2018.

727 Dickson, A. G.: An exact definition of total alkalinity and a procedure for the estimation of alkalinity and total
728 inorganic carbon from titration data. *Deep Sea Research Part A. Oceanographic Research Papers*, 28(6), 609–
729 623, 1981.

730 Dickson, A. G.: The development of the alkalinity concept in marine chemistry. *Marine Chemistry*, 40(1–2), 49–63,
731 1992.

732 Dickson, A.G.: Thermodynamics of the dissociation of boric acid in synthetic seawater from 273.15 to 318.15 K.
733 *Deep Sea Research Part A. Oceanographic Research Papers*, 37, no. 5: 755-766, 1990.

734 Dickson, A.G., Sabine, C.L., and Christian, J.R.: Guide to best practices for ocean CO₂ measurements. North Pacific
735 Marine Science Organization, 2007. Eisaman, M. D., Parajuly, K., Tuganov, A., Eldershaw, C., Chang, N.,
736 Littau, K. A. CO₂ Extraction from Seawater Using Bipolar Membrane Electrodialysis, *Energy Environ. Sci.*, 5:
737 7346. <https://doi.org/10.1039/c2ee03393c>, 2012.

738 Eisaman, M. D.; Rivest, J. L. B.; Karnitz, S. D.; De Lannoy, C.-F.; Jose, A.; DeVaul, R. W.; Hannun, K. Indirect
739 Ocean Capture of Atmospheric CO₂: Part II. Understanding the Cost of Negative Emissions. *International*
740 *Journal of Greenhouse Gas Control*, 70: 254–261, <https://doi.org/10.1016/j.ijggc.2018.02.020>, 2018.

741 Eisaman, M. D., Geilert, S., Renforth, P., Bastianini, L., Campbell, J., Dale, A. W., Foteinis, S., Grasse, P., Hawrot,
742 O., Löscher, C. R., Rau, G. H., and Rønning, J.: Assessing the technical aspects of ocean-alkalinity-
743 enhancement approaches, in: *Guide to Best Practices in Ocean Alkalinity Enhancement Research*, edited by:
744 Oschlies, A., Stevenson, A., Bach, L. T., Fennel, K., Rickaby, R. E. M., Satterfield, T., Webb, R., and Gattuso,
745 J.-P., Copernicus Publications, State Planet, 2-oae2023, 3, <https://doi.org/10.5194/sp-2-oae2023-3-2023>, 2023.

746 Eisaman, M. D.: Pathways for marine carbon dioxide removal using electrochemical acid-base generation, *Front.*
747 *Clim.*, 6, <https://doi.org/10.3389/fclim.2024.1349604>, 2024.

748 Feely, R.A., Alin, S., Carter, B., Bednaršek, N., Hales, B., Chan, F., Hill, T.M., Gaylord, B., Sanford, E., Byrne,
749 R.H., Sabine, C.L., Greeley, D., Juranek, L., Chemical and biological impacts of ocean acidification along the
750 west coast of North America, *Estuarine, Coastal and Shelf Science*, doi: 10.1016/j.ecss.2016.08.043, 2016.

751 Feng, E. Y., Koeve, W., Keller, D.P., and Oschlies, A.: Model-Based Assessment of the CO₂ Sequestration Potential
752 of Coastal Ocean Alkalinization. *Earth's Future*, 5, no. 12: 1252-1266, 2017.

753 Fennel, K., Long, M. C., Algar, C., Carter, B., Keller, D., Laurent, A., Mattern, J. P., Musgrave, R., Oschlies, A.,
754 Ostiguy, J., Palter, J., and Whitt, D. B.: Modeling considerations for research on Ocean Alkalinity Enhancement
755 (OAE), *State Planet Discuss.* [preprint], <https://doi.org/10.5194/sp-2023-10>, in review, 2023.

756 Ferderer, A., Chase, Z., Kennedy, F., Schulz, K.G., and Bach, L.T.: Assessing the influence of ocean alkalinity
757 enhancement on a coastal phytoplankton community. *Biogeosciences* 19, no. 23: 5375-5399, 2022.

758 Friis, K.; Körtzinger, A.; Wallace, D. W. R. The Salinity Normalization of Marine Inorganic Carbon Chemistry
759 Data. *Geophys. Res. Lett.*, 30 (2). <https://doi.org/10.1029/2002GL015898>, 2003.

760 Groen, A., Kittu, L., Ortiz Cortes, J., Schulz, K., and Riebesell, U.: Assessing the response of particulate organic
761 matter stoichiometry to ocean alkalination. *Ocean Visions Summit*, Atlanta, Georgia, USA,
762 2023ocvi.conf27171G. 4-6 April 2023

763 Hartmann, J., Suitner, N., Lim, C., Schneider, J., Marín-Samper, L., Arístegui, J., Renforth, P., Taucher, J., and
764 Riebesell, U.: Stability of alkalinity in ocean alkalinity enhancement (OAE) approaches—consequences for
765 durability of CO₂ storage. *Biogeosciences* 20, no. 4: 781-802, 2023.

766 Harvey, L.: Mitigating the atmospheric CO₂ increase and ocean acidification by adding limestone powder to
767 upwelling regions, *Journal of 640 Geophysical Research: Oceans*, 113, 2008.

768 He, J. and Tyka, M. D.: Limits and CO₂ equilibration of near-coast alkalinity enhancement, *Biogeosciences*, 20, 27–
769 43, <https://doi.org/10.5194/bg-20-27-2023>, 2023.

770 Ho, D. T., Bopp, L., Palter, J. B., Long, M. C., Boyd, P., Neukermans, G., and Bach, L.: Chapter 6: Monitoring,
771 Reporting, and Verification for Ocean Alkalinity Enhancement, *State Planet Discuss.* [preprint],
772 <https://doi.org/10.5194/sp-2023-2>, in review, 2023.

773 Ilyina, T., Wolf-Gladrow, D., Munhoven, G., and Heinze, C.: Assessing the potential of calcium-based artificial
774 ocean alkalization to mitigate rising atmospheric CO₂ and ocean acidification, *Geophysical Research Letters*,
775 40, 5909-5914, 2013.

776 IPCC: Summary for Policymakers. In: *Climate Change 2021: The Physical Science Basis, Contribution of Working*
777 *Group I to the Sixth Assessment Report of the Intergovernmental Panel on Climate Change*, edited by: Masson-
778 Delmotte, V., Zhai, P., Pirani, A., Connors, S. L., Péan, C., Berger, S., Caud, N., Chen, Y., Goldfarb, L., Gomis,
779 M. I., Huang, M., Leitzell, K., Lonnoy, E., Matthews, J. B. R., Maycock, T. K., Waterfield, T., Yelekçi, O., Yu,
780 R., and Zhou, B.: Cambridge University Press, Cambridge, United Kingdom and New York, NY, USA, 3–32,
781 <https://doi.org/10.1017/9781009157896.001>, 2022.

782 Isson, T. T., Planavsky, N. J., Coogan, L. A., Stewart, E. M., Ague, J. J., Bolton, E. W., et al.: Evolution of the
783 global carbon cycle and climate regulation on earth. *Global Biogeochemical Cycles*, 34, e2018GB006061.
784 <https://doi.org/10.1029/2018GB006061>, 2020.

785 Johnson, K.M., King, A.E., and Sieburth, J.M.: Coulometric TCO₂ analyses for marine studies: An introduction.
786 *Marine Chemistry* 16, pp. 61-82. 1985.

787 Jones, D.C., Ito, T., Takano, Y., and C.-W Hsu, C.-W.: Spatial and seasonal variability of the air-sea equilibration
788 timescale of carbon dioxide. *Global Biogeochemical Cycles*, 28(11), 1163–1178,
789 <https://doi.org/10.1002/2014GB004813>, 2014.

790 Khashgi, H. S.: Sequestering atmospheric carbon dioxide by increasing ocean alkalinity, *Energy*, 20, 915-922, 1995.

791 Köhler, P., Hartmann, J., and Wolf-Gladrow, D.A.: Geoengineering potential of artificially enhanced silicate
792 weathering of olivine. *Proceedings of the National Academy of Sciences* 107, no. 47: 20228-20233, 2010.

793 La Plante, E., Chen, X., Bustillos, S., Bouissonnie, A., Traynor, T., Jassby, D., Corsini, L., Simonetti, D., and Sant,
794 G.: Electrolytic seawater mineralization and the mass balances that demonstrate carbon dioxide removal. *ACS*
795 *EST Engg.* <https://doi.org/10.1021/acsestengg.3c00004>, 2023.

796 Lee, K., Kim, T.-W., Byrne, R.H., Millero, F.J., Feely, R.A., and Liu, Y.-M.: The universal ratio of boron to
797 chlorinity for the North Pacific and North Atlantic oceans. *Geochimica et Cosmochimica Acta* 74, no. 6: 1801-
798 1811, 2010.

799 Lewis, E., Wallace, D., & Allison, L. J.: Program developed for CO₂ system calculations.
800 <https://doi.org/10.2172/639712>, 1998.

801 Liu, X., Wang, Z.A., Byrne, R.H., Kaltenbacher, E.A., and Bernstein, R.E.: Spectrophotometric measurements of
802 pH in-situ: laboratory and field evaluations of instrumental performance. *Environmental Science & Technology*
803 40, no. 16, 5026-5044. 2006

804 Lu, X., Ringham, M., Hirtle, N., Hillis, K., Shaw, C., Herndon, J., Carter, B.R., and Eisaman, M.D.:
805 Characterization of an Electrochemical Approach to Ocean Alkalinity Enhancement. In *AGU Fall Meeting*
806 *Abstracts*, vol. 2022, pp. GC31C-01. 2022.

807 Lueker, T.J., Dickson, A.G., and Keeling, C.D.: Ocean pCO₂ calculated from dissolved inorganic carbon, alkalinity,
808 and equations for K₁ and K₂: validation based on laboratory measurements of CO₂ in gas and seawater at
809 equilibrium. *Marine chemistry* 70, no. 1-3: 105-119, 2000.

810 Minx, J.C., Lamb, W.F., Callaghan, M.W., Fuss, S., Hilaire, J., Creutzig, F., Amann, T., et al.: Negative
811 emissions—Part 1: Research landscape and synthesis. *Environmental Research Letters* 13, no. 6: 063001, 2018.

812 Montserrat, F., Renforth, P., Hartmann, J., Leermakers, M., Knops, P., and Meysman, F.J.R.: Olivine dissolution in
813 seawater: implications for CO₂ sequestration through enhanced weathering in coastal environments.
814 *Environmental Science & Technology* 51, no. 7: 3960-3972, 2017.

815 Moras, C.A., Bach, L.T., Cyronak, T., Joannes-Boyau, R., and Schulz, K.G.: Ocean alkalinity enhancement—
816 avoiding runaway CaCO₃ precipitation during quick and hydrated lime dissolution. *Biogeosciences* 19, no. 15:
817 3537-3557, 2022.

818 National Academies of Sciences, Engineering, and Medicine. A research strategy for ocean-based carbon dioxide
819 removal and sequestration. 2021.

820 National Academies of Sciences, Engineering, and Medicine. *Negative Emissions Technologies and Reliable*
821 *Sequestration: A Research Agenda*. 2018.

822 Nduagu, E. "Production of Mg(OH)₂ from Mg-silicate rock for CO₂ mineral sequestration. Dissertation for Abo
823 Akademi University, 2012.

824 Oschlies, A., Bach, L., Rickaby, R., Satterfield, T., Webb, R. M., and Gattuso, J.-P.: Climate targets, carbon dioxide
825 removal and the potential role of Ocean Alkalinity Enhancement, *State Planet Discuss.* [preprint],
826 <https://doi.org/10.5194/sp-2023-13>, in review, 2023.

827 Pierrot, D., Lewis, E., and Wallace, D.W.R.: MS Excel program developed for CO₂ system calculations.
828 ORNL/CDIAC-105a. Carbon Dioxide Information Analysis Center, Oak Ridge National Laboratory, U.S.
829 Department of Energy, Oak Ridge, Tennessee, 2006.

830 Rau, G.H.: Electrochemical splitting of calcium carbonate to increase solution alkalinity: Implications for mitigation
831 of carbon dioxide and ocean acidity. *Environmental science & technology* 42, no. 23: 8935-8940, 2008.

832 Renforth, P., and Henderson, G.: Assessing ocean alkalinity for carbon sequestration. *Reviews of Geophysics* 55,
833 no. 3: 636-674, 2017.

834 Rigopoulos, I., Harrison, A.L., Delimitis, A., Ioannou, I., Efstathiou, A.M., Kyratsi, T., and Oelkers, E.H. : Carbon
835 sequestration via enhanced weathering of peridotites and basalts in seawater. *Applied Geochemistry* 91: 197-
836 207, 2018.

837 Rueda, O., Mogollón, J.M., Tukker, A., and Scherer, L.: Negative-emissions technology portfolios to meet the 1.5°
838 C target. *Global Environmental Change* 67: 102238, 2021.

839 Rogelj, J., Popp, A., Calvin, K. V., Luderer, G., Emmerling, J., Gernaat, D., Fujimori, S., Strefler, J., Hasegawa, T.,
840 Marangoni, G., Krey, V., Kriegler, E., Riahi, K., van Vuuren, D. P., Doelman, J., Drouet, L., Edmonds, J.,
841 Fricko, O., Harmsen, M., Havlík, P., Humpenöder, F., Stehfest, E., and Tavoni, M.: Scenarios towards limiting
842 global mean temperature increase below 1.5 °C, *Nat. Clim. Change*, 8, 325–332, [https://doi.org/10.1038/s41558-](https://doi.org/10.1038/s41558-018-0091-3)
843 018-0091-3, 2018.

844 Schulz, K. G., Bach, L. T., and Dickson, A. G.: Seawater carbonate system considerations for ocean alkalinity
845 enhancement research, *State Planet Discuss.* [preprint], <https://doi.org/10.5194/sp-2023-12>, in review, 2023.

846 Shaw, C., Ringham, M.C., Lu, X., Carter, B.R., Eisaman, M.D., and Tyka, M.: Understanding the Kinetics of
847 Electrochemically derived Magnesium Hydroxide for Ocean Alkalinity Enhancement. In *AGU Fall Meeting*
848 *Abstracts*, vol. 2022, pp. GC32I-0713. 2022.

849 Song, S., Wang, Z.A., Gonnee, M.E., Kroeger, K.D., Chu, S.N., Li, D., and Liang, H.: An important
850 biogeochemical link between organic and inorganic carbon cycling: Effects of organic alkalinity on carbonate
851 chemistry in coastal waters influenced by intertidal salt marshes. *Geochimica et Cosmochimica Acta* 275:123-
852 139, 2020.

853 Suitner, N., Faucher, G., Lim, C., Schneider, J., Moras, C.A., Riebesell, U., and Hartmann, J.: Ocean alkalinity
854 enhancement approaches and the predictability of runaway precipitation processes- Results of an experimental
855 study to determine critical alkalinity ranges for safe and sustainable application scenarios. *EGU sphere*
856 [preprint], <https://doi.org/10.5194/egusphere-20223-2611>, 2023

857 Tyka, M.D., Arsdale, C.V., and Platt, J.C.: CO₂ capture by pumping surface acidity to the deep ocean. *Energy &*
858 *Environmental Science* 15, no. 2: 786-798, 2022.

859 Van Heuven, S., Pierrot, D., Rae, J., Lewis, E., & Wallace, D.: MATLAB program developed for CO₂ system
860 calculations. ORNL/CDIAC-105b, 530, 2011.

861 Vitillo, J. G., Eisaman, M.D., Aradóttir, E.S.P., Passarini, F., Wang, T., and Sheehan, S.W.: The role of carbon
862 capture, utilization and storage for economic pathways that limit global warming to below 1.5° C." *Iscience*:
863 104237, 2022.

864 Wang, H., Pilcher, D. J., Kearney, K. A., Cross, J. N., Shugart, O. M., Eisaman, M. D., & Carter, B. R.: Simulated
865 impact of ocean alkalinity enhancement on atmospheric CO₂ removal in the Bering Sea. *Earth's Future*, 11(1),
866 e2022EF002816, 2023

867 Wang, Z. A. and Cai, W. J.: Carbon dioxide degassing and inorganic carbon export from a marsh-dominated estuary
868 (the Duplin River): A marsh CO₂ pump. *Limnol. Oceanogr.* 49, 341–354, 2004.

869 Wolf-Gladrow, D. A., Zeebe, R. E., Klaas, C., Körtzinger, A., & Dickson, A. G.: Total alkalinity: The explicit
870 conservative expression and its application to biogeochemical processes. *Marine Chemistry*, 106(1–2), 287–
871 300, 2007.

872 Wurgaft, E., Steiner, Z., Luz, B., and Lazar, B.: Evidence for inorganic precipitation of CaCO₃ on suspended solids
873 in the open water of the Red Sea, *Marine Chemistry*, 186, pp. 145–155, 2016.

874 Wurgaft, E., Wang, Z., Churchill, J., Dellapenna, T., Song, S., Du, J., Ringham, M., Rivlin, T., and Lazar, B.:
875 Particle triggered reactions as an important mechanism of alkalinity and inorganic carbon removal in river
876 plumes, *Geophysical Research Letters*, 48, e2021GL093178, <https://doi.org/10.1029/2021GL093178>, 2021

877 Zeebe, R.E., and Wolf-Gladrow, D.: CO₂ in seawater: equilibrium, kinetics, isotopes. Vol. 65, Gulf Professional
878 Publishing. 2001.

879 Zhang, H., and Byrne, R.H.: Spectrophotometric pH measurements of surface seawater at in-situ conditions:
880 absorbance and protonation behavior of thymol blue. *Marine Chemistry* 52, no. 1, pp. 17-25. 1996